Article

Not peer-reviewed version

Ediacaran Fluviolacustrine Depositional Systems of the Amane n'Tourhart and Tifernine Basins (Anti-Atlas, Morocco): Facies Analysis, Petrography, Paleoenvironments, and Climatic–Volcanic Controls

Jihane Ounar *, Hicham El Asmi, Mohamed Achraf Mediany, Rachid Oukhro, Kamal Mghazli, James Pierce, David A. D. Evans, Malika Fadil, El Hassane Chellai, Moulay Ahmed Boumehdi, Nasrrddine Youbi, Timothy W. Lyons, Andrey Bekker

Posted Date: 2 February 2026

doi: 10.20944/preprints202602.0078.v1

Keywords: Anti-Atlas; Amane n'Tourhart and Tifernine sections; Ediacaran Ouarzazate group; fluviolacustrine systems; volcanism; climate fluctuations

 doi:10.20944/preprints202602.0078.v1

Article

Ediacaran Fluviolacustrine Depositional Systems of the Amane n'Tourhart and Tifernine Basins (Anti-Atlas, Morocco): Facies Analysis, Petrography, Paleoenvironments, and Climatic–Volcanic Controls

Jihane Ounar [1,*], Hicham El Asmi [2], Mohamed Achraf Mediany [1], Rachid Oukhro [1], Kamal Mghazli [1], James Pierce [3], David A.D. Evans [3], Malika Fadil [1], El Hassane Chellai [1], Moulay Ahmed Boumehdi [1,4], Nasrrddine Youbi [1,4,5], Timothy W. Lyons [6] and Andrey Bekker [6,7]

[1] Department of Geology, Faculty of Sciences-Semlalia, Cadi Ayyad University, Prince Moulay Abdellah Boulevard, P.O. Box 2390, Marrakech 40000, Morocco

[2] Department of Biology-Geology, Graduate Normal School of Bensouda, Sidi Mohamed Ben Abdellah University, Fez, Morocco

[3] Department of Earth and Planetary Sciences, Yale University, New Haven, CT 06511, USA

[4] Instituto Dom Luiz, Faculdade de Ciências, Universidade de Lisboa, 1749-016 Lisboa, Portugal.

[5] Faculty of Geology and Geography, Tomsk State University, 36 Lenin Ave, Tomsk, Russia.

[6] Department of Earth and Planetary Sciences, University of California, Riverside, CA 92521, USA

[7] Department of Geology, University of Johannesburg, Auckland Park, Johannesburg 2006, South Africa

* Correspondence: jihaneounar@gmail.com

Highlights

- Facies analysis documented thirteen facies that belong to three facies associations.
- Siliciclastic deposits record high-energy, fluvial channel and floodplain dynamics, whereas carbonate facies reflect shallow-water lacustrine conditions.
- Stromatolites and microbial mats indicate significant biogenic control on carbonate deposition.
- Facies associations record cyclic sedimentation governed by water-level fluctuations, alluvial-fan migration, and episodic lake expansion.

Deposition was controlled by paleoclimate variability and contemporaneous volcanic activity.

Abstract

This study integrates sedimentological and stratigraphic insights into the Ediacaran fluviolacustrine successions of the Amane n'Tourhart and Tifernine basins. The Amane n'Tourhart Basin developed within a caldera volcanic context, whereas the Tifernine Basin formed in a pre-caldera setting. These successions provide valuable information about the sedimentary processes operating in late Ediacaran continental environments. Field observations, facies analysis, and petrography reveal a variety of siliciclastic, carbonate, mixed siliciclastic- carbonate, and volcaniclastic facies. These facies form associations indicative of alluvial fan, floodplain, and shallow-water lacustrine settings. Alluvial fan deposits are dominated by conglomerates and sandstones forming braided systems. Fluviolacustrine sequences show a transition from clayey siltstones with calcareous nodules to nodular and massive limestones, marking a gradual shift from fluvial to lacustrine conditions. Laminated limestones and stromatolites indicate intermittent microbial activity that contributed to carbonate precipitation. Sedimentation was strongly influenced by volcanic inputs and climatic fluctuations, alternating between humid and arid conditions. These factors drove cycles of channel incision, sediment infill, and lake expansion–contraction, illustrating the dynamic interplay of tectonics, volcanism, and climate that modulated deposition in these Ediacaran terrestrial basins.

 doi:10.20944/preprints202602.0078.v1

Keywords: Anti-Atlas; Amane n'Tourhart and Tifernine sections; Ediacaran Ouarzazate group; fluviolacustrine systems; volcanism; climate fluctuations

1. Introduction

The Ediacaran Period (ca. 635–538 Ma), the final interval of the Neoproterozoic Era, represents a critical chapter in Earth history, marked by profound environmental, tectonic, geochemical, and biological transformations that set the stage for the Phanerozoic biosphere. It began with the termination of the Marinoan Snowball Earth glaciation, recorded globally by glacial diamictites and cap carbonates that reflect extreme climatic and carbon-cycle perturbations and major changes in ocean chemistry and redox conditions [1–5]. These environmental shifts coincided with the emergence and diversification of complex macroscopic life, notably the Ediacara biota, a diverse assemblage of soft-bodied organisms, that provides crucial insights to early multicellular eukaryotes and stem-group animals [6–8].

Simultaneously, the final breakup of Rodinia and the assembly of Gondwana strongly influenced basin development, sedimentation patterns, and ocean circulation, promoting widespread deposition of mixed carbonate–siliciclastic successions in Ediacaran basins worldwide [9,10]. The period is also characterized by large-amplitude carbon isotope excursions, which serve as key chemostratigraphic markers and reflect dynamic interaction among tectonics, climate, ocean redox state, and biological productivity [11,12]. Despite significant advances, the Ediacaran remains one of the least understood intervals of Earth history, and integrated stratigraphic, sedimentological, paleontological, and geochemical studies are essential to constrain the timing, drivers, and consequences of early animal evolution and Earth System reorganization.

The Anti-Atlas Belt of Morocco provides an exceptional record of the Ediacaran Period, preserving one of the most complete and accessible Neoproterozoic successions along the northern margin of the West African Craton. It hosts key paleontological and sedimentological archives, including microbialites, microbially induced sedimentary structures (MISS) and soft-bodied Ediacaran fossils, offering valuable insights into the environmental context of early multicellular life along the peri-Gondwanan margin [13–16]. Owing to its stratigraphic continuity and well-preserved records, the Anti-Atlas Belt constitutes a reference region for studying the interactions among tectonics, climate, ocean chemistry, and biological innovation during the Ediacaran.

Although Ediacaran life is primarily recorded in marine carbonate and siliciclastic successions, relatively little is known about the terrestrial counterparts of these environments. Only rare locations worldwide preserve Ediacaran sections deposited in fluvial and lacustrine settings, including the sedimentary successions of the Amane-n'Tourhart and Tifernine localities (Ouarzazate Group) in the Anti-Atlas Mountains of southern Morocco. Despite some previous work [17–27] these sections have received limited attention regarding their sedimentology and facies architecture.

A comprehensive investigation of these sections is critical to place them within the temporal and spatial framework of the Ediacaran. The present study aims to develop a temporally calibrated record of depositional settings, paleogeography, and life habitats in the mid–late Ediacaran terrestrial sedimentary successions of the Quarzazate Group. Sedimentology and facies analyses were applied to characterize depositional environments and diagenetic processes.

Previous depositional models for the Amane-n'Tourhart and Tifernine basins are oversimplified and lack detailed consideration of vertical and lateral facies variations, paleocurrent trends, and the role of microbial mats in sedimentary dynamics. In this context, the present study integrates sedimentological, stratigraphic, and paleocurrent analysis of five measured sections to refine depositional models and assess fluviolacustrine dynamics along the northern margin of the West African Craton during the mid-to-late Ediacaran. Fluviolacustrine dynamics has been controlled by a complex and evolving interaction between rivers and lakes, where river inflow, lake-level fluctuations, and climatic and tectonic controls produced diverse deposits—including those of deltas and mudflats, with sediments of varying grain size (clay, silt, sand), often modulated by wet/dry

 doi:10.20944/preprints202602.0078.v1

cycles. These Ediacaran terrestrial systems are crucial for reconstructing continental paleoenvironments and understanding life habitat in such settings.

2. Geological Setting

The Anti-Atlas Belt, located in southern Morocco along the northern margin of the West African Craton (WAC) (Figure 1 (a) and (b)), represents a major segment of the Pan-African (883 - 541Ma) orogenic system. It is composed of Paleoproterozoic to Neoproterozoic basement rocks, locally uplifted to altitudes exceeding 1 km due to Cenozoic tectonic events [28,29]. These basement rocks are unconformably overlain by a thick, relatively undeformed succession of Ediacaran to early Paleozoic volcanic, volcaniclastic, and sedimentary sequences, most notably the Ouarzazate Group [21,30,31]. The Anti-Atlas inliers expose numerous, mainly WSW–ENE trending units, where the Ouarzazate Group forms an extensive volcanics-dominated succession recording subaerial volcanism and sedimentary processes [21,31,32]. A detailed overview of the regional geology of the Anti-Atlas Belt is provided by [31,33–35], whereas the lithostratigraphic framework of the Ediacaran succession was most recently described by [15].

The Ouarzazate Group ("PIII" or XIII of Choubert [36]) is a significant Proterozoic lithostratigraphic unit of the Anti-Atlas Belt formed during the late Ediacaran period (590-543 Ma). It includes extensive volcanic as well intrusive rocks associated with the early stage in the Iapetus Ocean opening. It belongs to the Central Iapetus Magmatic Province (CIMP), and covers a vast area of ~2 × 10^6 km^2, with thickness locally exceeding 2.5 km and an estimated magmatic volume of ~1 × 10^6 km^3 [33,37–41]. Lithologically, it is dominated by densely welded ignimbrites, tuffs, and lava flows, ranging from andesitic basalts to rhyolites in composition, with high-K, calc-alkaline to tholeiitic affinities [21,34,39,40,42]. The Ouarzazate Group was not affected by the main Pan-African deformation at ca. 647 Ma and was deposited on a highly differentiated basement topography, which, coupled with the large and rapid variations in thickness of the Ouarzazate Group itself, strongly suggests that this group was deposited in an extensional/transtensional setting [38,43,44]. The Ouarzazate Group magmatism has been attributed to either continental arc volcanism and eventual slab break-off that resulted in asthenospheric upwelling, or a mantle plume activity [21,31,33,39,41,44–48]. Geochronological data constrain the earliest Ouarzazate Group volcanism to 590 - 588 Ma, whereas the termination of rift-related volcanism is nearly synchronous across the Anti-Atlas Belt at 561 - 543 Ma [21,31,34,39,40,46,48,49]. The Ouarzazate Group calderas with large volumes of pyroclastic flow deposits (ignimbrites) and ash falls extensively developed over the large part of the Anti-Atlas Belt [21,42,44,50,51].

The Oued Dar'a Caldera, located southwest of the Saghro Massif, is a large, rectangular volcanic depression (~11 × 18 km) infilled with densely welded rhyolitic to dacitic ash-flow tuffs [21,40]. The caldera formed along a northeast-trending left-lateral strike-slip fault system and is bounded by major strike-slip faults [21]. Preserved intra-caldera fill locally exceeds 500 m in thickness, with an estimated eruptive volume of 100–200 km^3, consistent with caldera-scale ignimbrite accumulation [52,53]. The southwestern margin is characterized by coarse-grained volcaniclastic deposits interbedded with lacustrine beds containing microbialites [17–22,24–27,42]. The Tizgui area (Figure 1 (c)) forms part of this caldera and exposes well-preserved volcanic and volcanosedimentary deposits within the Oued Dar'a Volcanic Complex [21,40].

Two study areas were targeted, Amane-n'Tourhart and Tifernine sections (Figures 1 (c), (d) and (e)). They are located along the western margin of the Saghro Inlier, the type locality of the Ouarzazate Group [19]. The Amane-n'Tourhart section is located between the villages of Amane–Issougri and Ait Saoun along the Ouarzazate–Agdz Road at the 464 km sign (Ouarzazate–Alougoum 1:100,000 and Tizgui 1:50,000 map sheets) and has been a classical stop for multiple geological field excursions [19,54]. The Tifernine section lies ~8 km southwest of Ait Saoun and it is separated from the Amane-n'Tourhart section by the younger Adoudou Formation [19,31,55].

The Amane-n'Tourhart sequence (Figure 1 (d)) forms a lenticular unit approximately 1 km long and ~30 m thick, resting unconformably on a succession of andesitic lava flows and associated

 doi:10.20944/preprints202602.0078.v1

pyroclastic rocks. The unit is slightly folded and faulted and consists of fluviolacustrine and volcano-sedimentary deposits, including peperites and andesitic breccias at the top, associated with post-caldera volcanic units of the Oued Dar'a Caldera [40]. Choubert [17]first proposed a lacustrine origin for these meter-thick carbonate deposits, formed contemporaneously with volcanic activity, an interpretation later confirmed and refined by [30,54]. Structural observations indicate that tectonics did not exert a primary control on sedimentation. However, several faults affected the unit after or during deposition. An approximately W–E-trending fault exposed at the level of the Oued is interpreted as syn-depositional, whereas a subvertical NE–SW-oriented fault with a steep SE dip cuts the central part of the succession (Figure 1 (d)), affecting both stromatolitic (Ls2, Ls3) and associated carbonate facies (Fm1, Ln, Lm). An additional NW–SE-trending fault, inferred near the roadway (Figure 1 (d)), is considered post-depositional. The succession also displays soft-sediment deformation structures, including large-amplitude folds affecting sandstone beds (Sm) overlying the Lm carbonates. These beds locally exhibit a dish-shaped geometry in the central part of the unit, truncated by the NE–SW fault (Figure 1 (d)).

The Tifernine sequence of the Ouarzazate Group (Figure 1 (e)) similarly consists of lenticular lacustrine deposits concordant with andesitic lava flows at the base and overlain by porphyritic andesitic lavas [30,31]. Although Álvaro [20] initially suggested that the Tifernine section was stratigraphically higher than Amane-n'Tourhart, recent U–Pb zircon geochronology demonstrates that the Amane-n'Tourhart succession is slightly younger (564–561 Ma), whereas the Tifernine deposits predate ~566 Ma and postdate ~590 Ma [40,47,48], in agreement with regional 1:50,000 geological mapping of the Bou Azzer area [56,57]. In the Tifernine area, the carbonate succession (Ll/Fm2) forms a monoclinal structure dipping toward the SE and is affected by post-depositional dextral strike-slip faults observed along the Oued de Tifernine (Figures 1 (e) and 11 (d)).

These studied sequences that cover a period between 590 Ma and 561 Ma provide critical insights into sedimentary deposition in close association with Ediacaran volcanic activity, allowing detailed reconstruction of volcano-sedimentary dynamics at the western border of the Saghro Inlier and within the context of large-scale, caldera-related volcanism in the Ouarzazate Group. These sequences also represent a largely unexplored archive of the terrestrial Ediacaran environments.

 doi:10.20944/preprints202602.0078.v1

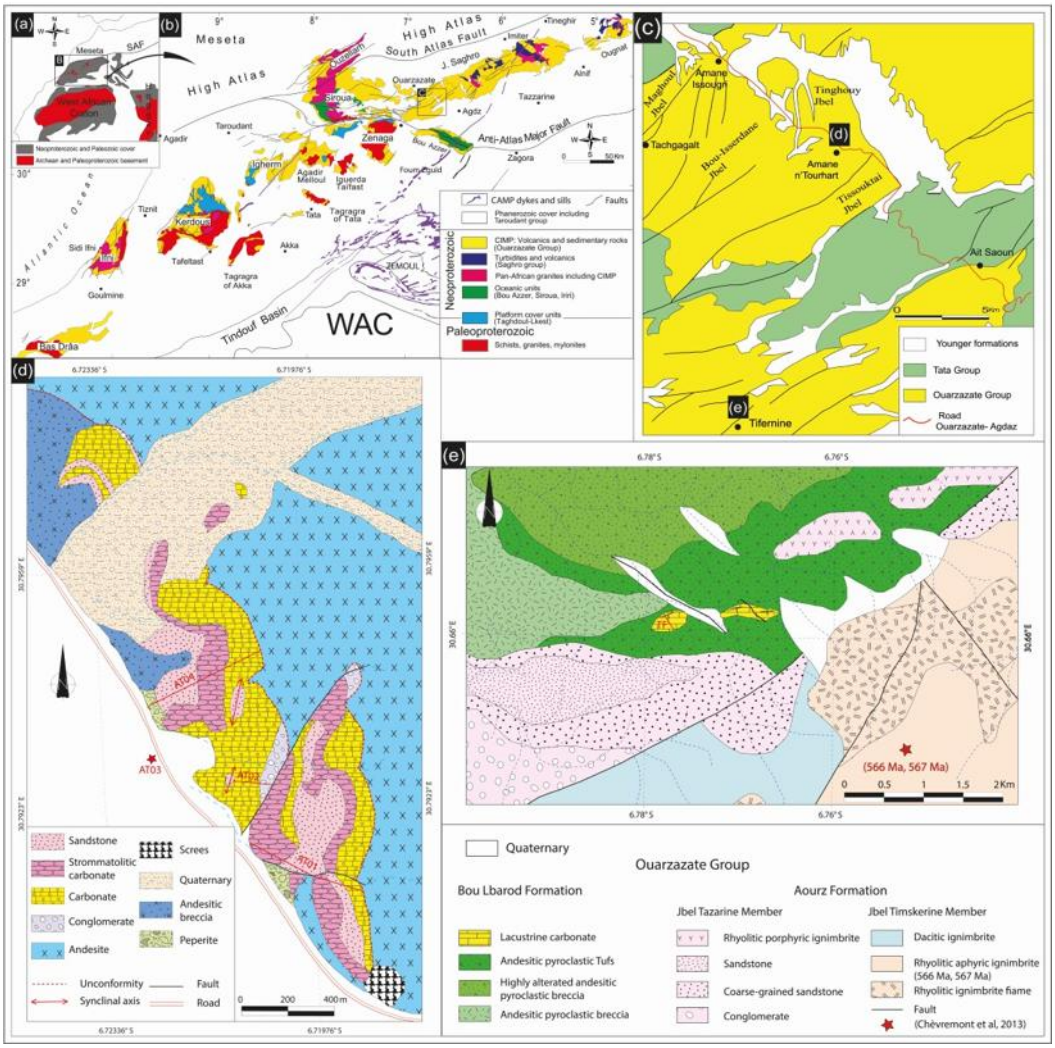

Figure 1. (a) The Anti-Atlas Belt at the northern margin of the West African Craton (WAC); (b) Geological map of the Anti-Atlas Belt in southern Morocco modified after Gasquet and Ait Lahna [33,35]; (c) Geological map of the western Saghro with location of Amane-n'Tourhart and Tifernine study areas (modified from Álvaro [20]); (d) Geological map of the Amane n'Tourhart area (this study); (e) Geological map of the Tifernine area modified from the Bou Azzer 1:50,000 geological map [56,57].

3. Materials and Methods

Given depositional facies with fluctuating accommodation space (e.g., lakes or seas), a detailed lithostratigraphic, sedimentological a petrographic analysis was carried out. This involved reconstruction of depositional environments and hydrodynamic conditions, and controls of paleoclimate and tectonics on sedimentation. Both fieldwork and laboratory analysis were performed in this study.

3.1. Fieldwork

Two study areas, Amane n'Tourhart and Tifernine, were selected in the southern Saghro Inlier based on field data (Figure 1 (b)). While sharing lithostratigraphic, sedimentological, petrographic, tectonic, and volcanic similarities that enable correlations, each area exhibits distinct characteristics. The study sections were logged in detail for their lithostratigraphy and sedimentology at both large and small scales. Conventional lithofacies analysis was included to document facies based on their geometry, thickness, lithology, sedimentary structures, grain size, and composition of the matrix. The fieldwork led to logging with a Jacob's staff of four lithostratigraphic sections in the Amane n'Tourhart area (AT01, AT02, AT03, AT04) (Figure 2) and one in the Tifernine area (TF) (Figure 3).

 doi:10.20944/preprints202602.0078.v1

The necessity for 4 logged sections in the Amane n'Tourhart area is due to its lithological complexity. Tifernine, on the other hand, is lithologically homogeneous (Figures 1 (e) and 4). These spatially separated and more or less complementary sections have enabled us to establish lithostratigraphy of these Ediacaran fluvio-lacustrine deposits. As a result, fifteen facies were identified in the study areas. These facies were further subdivided on the basis of their genetic typology. Over 90 samples were studied and analyzed in the laboratory for texture, structure, and mineralogy.

The results of the facies analysis of the Amane n'Tourhart and Tifernine successions are illustrated in Table 1. Lithofacies types were grouped into lithofacies associations taken in consideration the stratal stacking patterns and depositional environments. The facies associations include alluvial fan, floodplain, and shallow-water, lacustrine deposits.

3.2. Laboratory Work

The work began with the preparation of more than 30 thin sections at the Geology Department of the Faculty of Sciences Semlalia (Marrakesh, Morocco) and the Earth and Planetary Sciences Department of University of California Riverside (USA). We performed a petrographic study and digital microphotography on these sections using an Olympus polarizing microscope at the Faculty of Sciences Semlalia, Marrakesh (FSSM), Department of Geology. Other laboratory analyses were conducted at "The City of Innovation" (a research center attached to the University Sidi Mohamed Ben Abdellah of Fez). These analyses included the study of microtextures and microstructures using a Scanning Electron Microscope (SEM). Selected carbon-coated thin sections were examined using secondary electron (SE) and back-scattered electron (BSE) imaging with a JEOL JSM-IT500HR SEM. The instrument is equipped with a Schottky field-emission gun (FEG) that provides high beam brightness and long-term stability. The microscope was operated at beam currents of 10–20 nA and accelerating voltages ranging from 0.5 to 30 kV, allowing optimization of imaging conditions for both surface morphology (SE mode) and compositional contrast (BSE mode). The high brightness and probe current stability of the Schottky FEG enabled high-resolution imaging and reliable analytical performance, particularly for mineralogical and microtextural investigations.

We also used the Stereonet v. 11 program, which can be openly accessed on https://www.rickallmendinger.net/, to analyze the elongation of columnar stromatolites and pebbles of conglomerates, and the orientation of ripple marks.

4. Results

In the Amane n'Tourhart area, four detailed stratigraphic logs were measured along sections AT01, AT02, AT03, and AT04 (Figure 2) to document the vertical and lateral organization of lithofacies, which exhibits a high degree of heterogeneity. Sections AT01 and AT04 record a complete sequence from the underlying andesites at the base to the brecciated andesites at the top, whereas AT02 and AT03 are incomplete due to faulting, folding, and minor shear zones. The succession can be divided into a lower part, approximately 11 m thick, composed of clayey siltstone with calcite nodules (Fm1), nodular limestones (Ln), massive limestones (Lm), and massive limestone with scattered clasts (Lmc), with occasional intercalations of massive siltstone-mudstone (Fm2), forming a relatively continuous interval with minor variations in thickness; and an upper part, about 15 m thick, consisting of massive sandstone (Sm), horizontally bedded sandstone (Sh), matrix-supported conglomerates (Gmm), clast-supported conglomerates (Gcm), and stromatolitic limestones (Ls1, Ls2, Ls3), which exhibits more complex internal architecture and minor lenticular intercalations, resulting in a total thickness of roughly 26 m. Section AT02 corresponds primarily to the lower part, whereas section AT03 represents mainly the upper part, while AT01 and AT04 preserve both parts in their entirety, allowing a detailed analysis of the vertical arrangement and lateral variations in lithofacies. In the Tifernine area, a single, laterally continuous section was measured (Figure 3) with a total thickness of 40 m, composed of laminar limestone (Ll) and massive siltstone-mudstone (Fm2), showing regular alternations and consistent thickness along the outcrop. Together, these

 doi:10.20944/preprints202602.0078.v1

lithostratigraphic observations provide a comprehensive framework for the detailed facies analysis presented below.

4.1. Facies Analysis

Facies analysis and interpretations were performed based on lithologies, sedimentary structures and textures, as well as allochemical and orthochemical compositions observed in the field and imaged in the laboratory, leading to the identification of fifteen distinct facies grouped into three main categories. The clastic or detrital facies group comprises conglomerates, sandstones, and muddy siltstones, representing the detrital components of the succession. The carbonate facies group includes massive, laminar, nodular, and stromatolitic limestones, distinguished by the presence or absence of sedimentary structures and forming intervals with variable resistance to erosion, which affects their expression in the landscape. The mixed facies group consists of nodular carbonates with silty grains and limestones containing quartz grains and pebbles, representing transitional facies between detrital and carbonate facies groups. In addition to these sedimentary facies groups, a fourth group of volcanic facies was identified, varying by area: in the Amane n'Tourhart area, dacitic andesite underlies the fluviolacustrine deposits, which are in turn capped by andesitic breccia, whereas in the Tifernine area, microlitic andesite underlies the carbonate succession and rhyolite are developed at the top of the carbonate succession.

 doi:10.20944/preprints202602.0078.v1

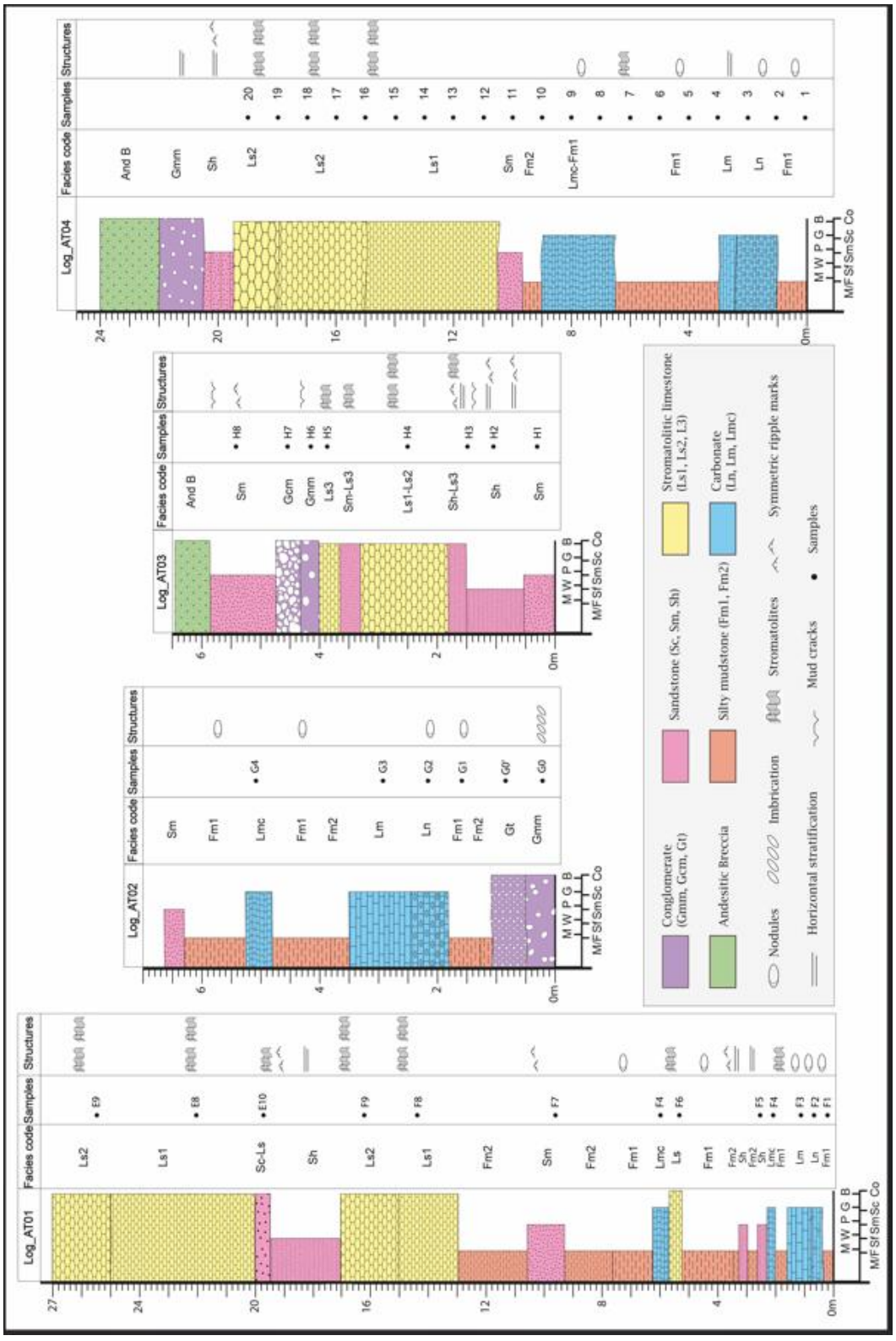

Figure 2. Lithostratigraphy of the Amane n'Tourhart area showing four measured logs with different facies: siliciclastic facies including conglomerate (Gmm, Gcm, Gt), sandstone (Sm, Sh), and silty mudstone (Fm2); carbonate facies (Ln, Lm); mixed facies (Fm1, Lmc, Ls); and volcanic facies (And).

 doi:10.20944/preprints202602.0078.v1

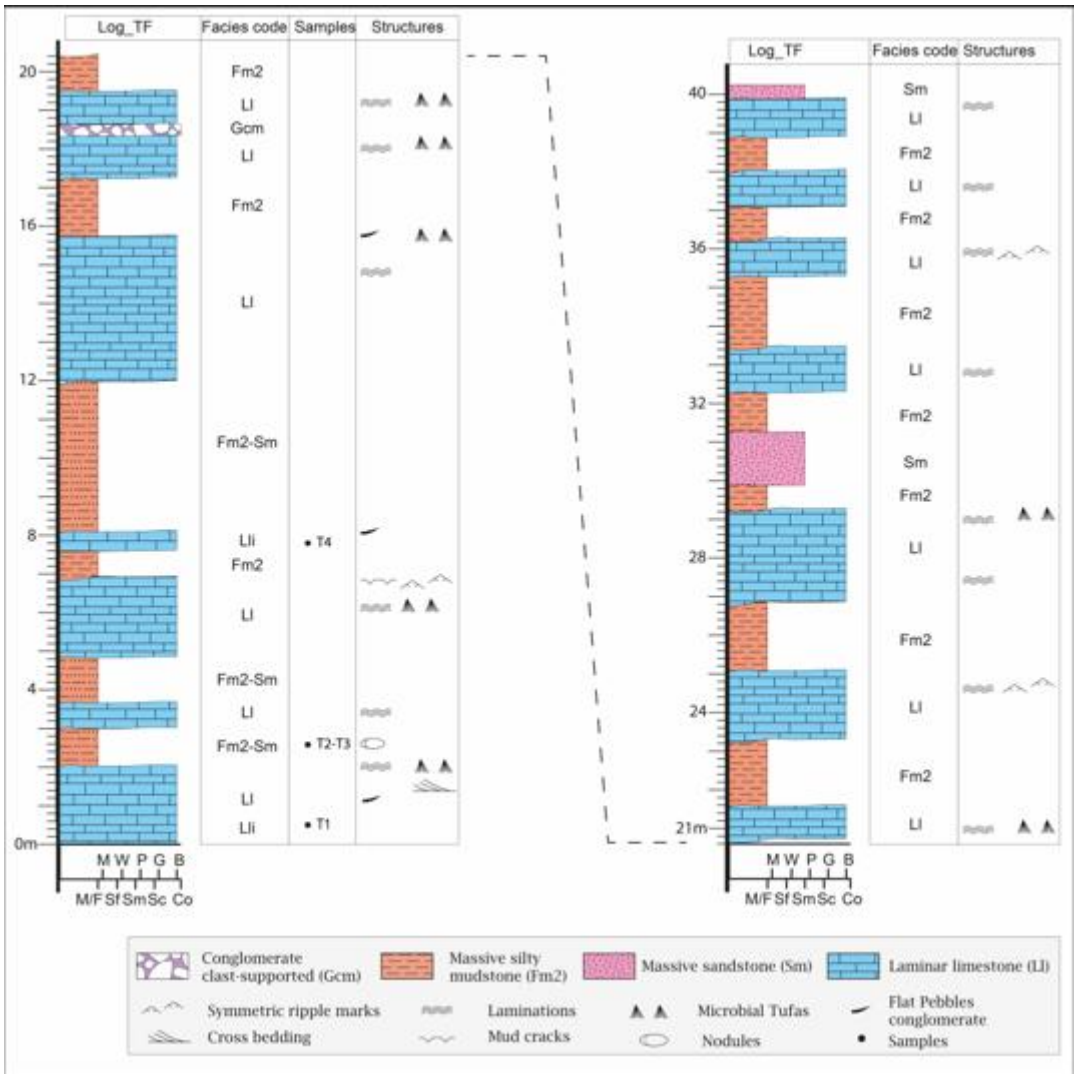

Figure 3. Lithostratigraphy of the Tifernine area showing one measured section with different facies: siliciclastic facies, including conglomerate (Gcm), massive sandstone (Sm), and massive silty mudstone (Fm2), and carbonate facies (Ll, Lli).

Table 1. Fluviolacustrine facies of the of Amane n'Tourhart and Tifernine area.3.1.1. Subsubsection

Facies	Lithology	Sediment characteristics	Geometry / Thickness	Interpretation	Figure
Gmm1	Matrix-supported conglomerate. Volcaniclastic conglomerate (peperite).	Sub-rounded andesitic clasts in reddish sandstone matrix; poorly sorted; mudcracks on tops; gradational contacts	Flat to lenticular beds, ~25 cm thick	Volcano-sedimentary deposit (peperite) formed by lava–sediment interaction	Figures 3 (a)–(b), 5 (c)–(e), (g)
Gmm2	Matrix-supported conglomerate.	Sandstone and siltstone clasts, sub-angular to sub-rounded, oriented NE–SW, poorly sorted	Lenticular, channel-shaped base, ~30 cm thick	Deposition by migrating 3D dunes or longitudinal bars within fluvial channels	Figures 3 (a)–(b), 5 (b)
Gcm	Clast-supported conglomerate.	Poorly sorted, sub-rounded clasts (mm–cm in size), volcanic or carbonate depending on site	Tabular/lenticular bodies, 0.2–0.25 m thick	Hyperconcentrated flood flow or debris flow deposit	Figures 5 (c) – (d)

 doi:10.20944/preprints202602.0078.v1

Gt	Cross-bedded conglomerate	Trough cross-bedding, scoured base, upward fining, mixed detrital grains	Lenticular 0.6 m thick	Channel-fill deposits formed by high-velocity river flows	Figures 3 (a)–(b), 5 (a), (h)
Sm	Massive sandstone	Massive, pink to purple, locally silicified, normal grading, no sedimentary structures	Lenticular; 0.2–2 m thick	Rapid deposition from high-energy flows in channels or lateral bars	Figures 3 (a)–(b), 6 (a)–(h)
Sh	Planar bedded sandstone	Planar bedding, iron-rich and detrital alternations, ripple marks	Tabular/lenticular, decimetric–metric	Tractional deposits under upper flow regime in channels, flood-related	Figures 3 (a)–(b), 6 (b)–(j)
Fm2	Massive, silty mudstone	Highly friable, non-erosive base, fine-grained	Tabular/lenticular, 0.15–4 m thick	Suspension fallout during waning floods (final stage in turbidite deposition)	Figures 3 (a)–(b), 5
Lm	Massive limestone	Sparitic to micro-sparitic calcite, spherulitic, partially silicified	Tabular/lenticular, up to 1 m thick	Lacustrine to deep-water, fluviolacustrine carbonate deposition	Figures 3 (a)–(b), 7 (a)–(b), (d), (i)
Ln	Nodular limestone	Alternating micritic and detrital lamina, spherulitic and stromatolitic textures	Lenticular/tabular, 0.25–1.25 m thick	Transitional facies between fluvial (Fm1) and lacustrine (Lm) facies	Figures 3 (a)–(b), 7 (c), (h)
Ll	Laminar limestone	Horizontal or inclined microbial lamina, mudcracks, ripple marks, MISS	Tabular/lenticular, 0.5–4 m thick	Shallow-water, lacustrine environment with periodic emersion	Figures 5, 8 (a)–(h), 9 (a)–(g)
Fm1	Massive silty mudstone with limestone nodules	Red–purple siltstone with white carbonate nodules, microsparitic to sparitic calcite	Tabular/lenticular, 0.3–3.5 m thick	Flood-plain environment with fluvial channels, transitional to carbonates	Figure 3 (a)–(b), 7 (a)–(b), (g)
Lmc	Massive limestone with scattered clasts	Limestone with detrital quartz, plagioclase, and iron oxides	Lenticular, 0.2–0.35 m thick	Deposition in relatively deep lacustrine setting with increasing energy upsection	Figures 3 (a)–(b), 7 (e)–(f), (j)
Ls1	Inclined, columnar stromatolitic limestone	Alternating red detrital and white carbonate lamina; inclined columns	Biohermal; up to 5 m thick	Formed in high-energy, submerged environment in the lake	Figures 3 (a)–(b), 10 (a)–(c), 12 (b)–(c)
Ls2	Domal stromatolitic limestone	Linked vertical domes up to 80 cm in diameter, red–white alternations	2 m thick	Formed in aquatic settings with laminar flow (palustrine or low-energy riverbeds)	Figure 10 (e)–(g), 12 (d)–(f)
Ls3	Planar laminated stromatolitic limestone	Alternating red–white lamina; micro-domal to planar structures, silicified	0.3 m thick	Shallow-water lacustrine stromatolites	Figure 10 (h)–(j), 12 (a)–(f)
Volcanic facies	Andesites, Breccia andesites, Rhyolites	Porphyritic texture, altered plagioclase, pyroxene, quartz in microlitic matrix	—	Volcanic unit (pre and post-caldera stage), underlying	Figure 11 (a)–(d)

 doi:10.20944/preprints202602.0078.v1

	sedimentary succession

4.1.1. Siliciclastic Facies

Siliciclastic facies have been described and interpreted from the coarsest (conglomerates) to the finest (silty mudstone). In the following description, the letters are used as follows: G (Gravel) for conglomeratic facies, S (Sand) for sandstones, and F (Fine) for siltstones and mudstones.

F1: Matrix-Supported Conglomerates (Gmm)

Description: This facies is absent in the Tifernine area, but occurs at Amane n'Tourhart (Figure 1 (d); Figure 2), where it forms continuous to lenticular layers and is represented by two distinct types. The first type (Gmm1; Figures 2 (b); 4 (c) and (d)), about 25 cm thick, is interpreted as a volcanosedimentary deposit (peperite). It is composed of sub-rounded to poorly sorted volcanic (andesitic) fragments dispersed within a reddish to violet sandstone matrix, with mudcracks visible at the top of the bed (Figure 4 (e)). Microscopically, it consists of large pyroclastic, andesitic clasts embedded in a sandy matrix composed of quartz and plagioclase grains, showing no sharp contrast between the clasts and the matrix (Figure 4 (g)). The second type (Gmm2; Figures 2 (b); 4 (b)), approximately 30 cm thick, displays a channel-shaped erosive base and contains a sandstone–limestone matrix with sandstone and siltstone clasts. These clasts are oriented and imbricated towards the southwest (NE–SW orientation), ranging from sub-rounded to angular and varying in size from millimeters to centimeters.

Interpretation: Facies Gmm1 is interpreted as peperitic deposits formed by the interaction between hot, andesitic magma and unconsolidated, water-saturated sediments. Mingling of fresh volcanic fragments with the sedimentary matrix, together with the absence of sharp boundaries, indicates a syn-eruptive magma-sediment interaction typical of shallow subaqueous or marginal lacustrine environments [58–60]. The development of mudcracks at the top of the bed suggests subaerial exposure subsequent to emplacement. In contrast, facies Gmm2 represents a channelized deposit generated by tractional currents within a confined fluvial or deltaic setting [61]. The erosive base, internal cross-bedding, and upward decrease in grain size indicate deposition during the migration of three-dimensional dunes or longitudinal bars under waning flow conditions.

F2: Clast-supported conglomerate (Gcm)

Description: This facies is characterized by a high proportion of clasts relative to the matrix, with the clasts embedded within the matrix. The matrix composition varies: at Amane n'Tourhart, it consists of sandstone (Figures 4 (c) and (d)), while in Tifernine, it is limestone (Figure 4 (f)). The facies forms tabular or lenticular bodies with bases that are either gullied or flat, with thicknesses ranging from 0.25 m (Amane n'Tourhart) (Figure 2) to 0.2 m (Tifernine) (Figure 3) and lateral extension on a meter scale. The clasts are subrounded, with size ranging from millimeters to centimeters. The clasts' composition differs depending on the matrix. In the Amane n'Tourhart area, they are volcanic (andesitic) and fresh, interpreted as peperite (volcanosedimentary rock) (Figures 4 (c) and (d)). In Tifernine, the clasts are carbonate, primarily limestone (Figure 4 (f)).

Interpretation: Facies Gcm reflects contrasting depositional processes between the two areas. At Amane n'Tourhart, it is interpreted as a peperitic facies formed through direct interaction between andesitic lava and unconsolidated, water-saturated sediments, producing in situ fragmentation and mingling of magma and sediment. This interpretation is supported by the presence of fresh volcanic clasts embedded with a detrital matrix, typical of magma–sediment mingling in shallow, subaqueous environments [58–60]. In contrast, the Gcm facies in the Tifernine area, characterized by carbonate clasts in a calcareous matrix, is interpreted as a product of short-lived, high-energy sedimentary reworking along a shallow lacustrine margin, resulting in local erosion and redeposition of carbonate beds [62,63]. Overall, this facies records syn-eruptive peperitic processes at Amane n'Tourhart and

 doi:10.20944/preprints202602.0078.v1

reworking of carbonate material at Tifernine, illustrating the interplay between volcanic activity and sedimentation within the basin.

F3: Cross-stratified conglomerate (Gt)

Description: Positioned above facies Gmm (the second type) (Figures 2 (b), 4 (a)), this facies measures 0.6 m in thickness and features coarse-grained clasts at the base, which become more abundant towards the top, but decrease in size, forming a microconglomeratic texture. The clasts range from centimeter to millimeter in size. This facies is distinguished by a scoured base and trough cross-bedding. Its matrix consists of limestone. Microscopically, this facies is composed of sub-angular grains of quartz, plagioclase, calcite, sandstone, and andesite, set in a micritic to microsparitic matrix (Figure 4 (h)).

Interpretation: Facies Gt is interpreted as a minor channel-fill deposit within fluvial systems, formed under high-energy conditions in the deepest section of the channel. The development of scoured base and trough cross-bedding indicates deposition from concentrated; high-velocity flows capable of transporting coarse-grained clasts, with the upward fining reflecting waning flow energy during deposition [64–66]. The mixed composition of clasts suggests derivation from multiple upstream sources, including both volcanic and detrital materials, while embedding with a micritic to microsparitic matrix points to rapid deposition with limited reworking.

 doi:10.20944/preprints202602.0078.v1

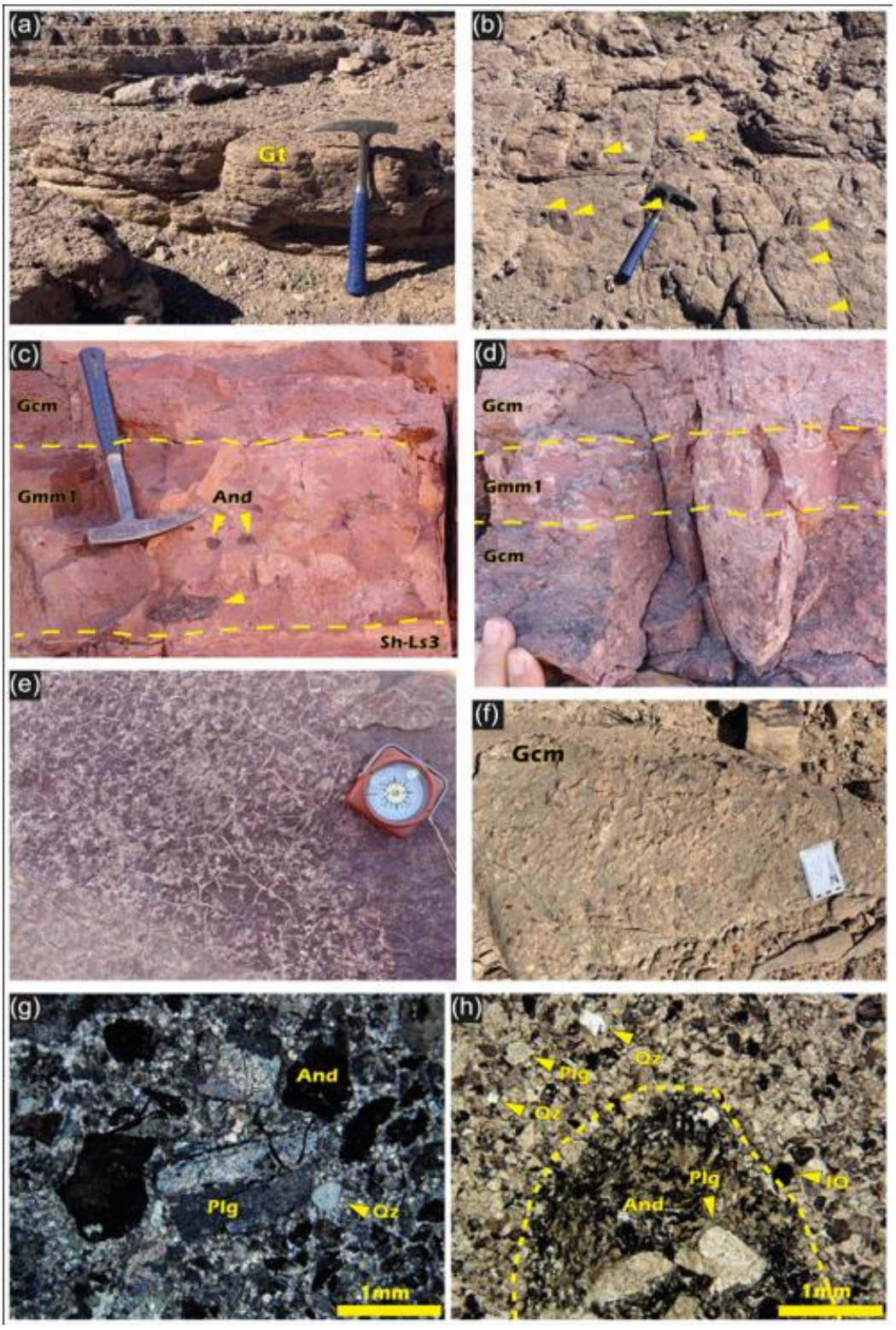

Figure.4. Field and microscopic photographs of conglomeratic facies; (a) Cross-stratified conglomerate (Gt); (b) Matrix-supported conglomerate (Gmm2) characterized by oriented sandstone pebbles; (c)-(d) Matrix-supported conglomerate (Gmm1) containing andesite blocks (volcanosedimentary facies interpreted as peperites) with clast-supported conglomerate (Gcm); (e) Mudcracks developed at the top of the Gmm1 bed; (f) Clast-supported conglomerate (Gcm) in the Tifernine area; (g) Photomicrograph in cross-polarized light of facies Gt; (h) Photomicrograph in cross-polarized light of facies Gmm1 (Peperite) (Qz: Quartz, Plg: Plagioclase, And: Andesite, IO: Iron Oxide).

F4: Massive sandstone (Sm).

 doi:10.20944/preprints202602.0078.v1

Description: This facies forms lenticular beds 0.2–2 m thick, with a non-erosive base and lateral extent ranging from decimeters to meters (Figures 2, 5). It comprises massive sandstones exhibiting normal grading from coarse-grained sandstone at the base to fine-grained sandstone and massive siltstone and mudstone at the top, sometimes silicified, particularly in AT03. Coarse-grained sandstones contain sub-angular to sub-rounded quartz and plagioclase grains, altered andesite fragments, and opaque minerals such as hematite and magnetite, cemented with micritic limestone or silica. Fine-grained sandstones contain more abundant matrix and are poorly sorted. Plagioclase grains show partial alteration to secondary minerals such as chlorite. In the Tifernine area, above laminated limestone (Ll), a friable, massive arkosic sandstone (Sm) occurs with altered plagioclase grains less than 1 mm in size and andesitic rock fragments in a sparse clay and iron-oxide matrix (Figures 4, 7 (c)).

Interpretation: The massive sandstone facies (Sm) is interpreted as deposits from channels and/or lateral accretion, formed by rapid accumulation from bedload and/or suspended load transported by high-energy flows during floods [67–69]. Normal grading from coarse- to fine-grained material and the absence of well-developed sedimentary structures suggest a high sedimentation rate under a shallow, high-energy flow regime, where suspended solids settled rapidly [70,71]. This facies reflects episodic, high-energy fluvial processes capable of transporting both coarse- and fine-grained detrital material, including volcanic fragments and altered plagioclase grains, within confined channels or along lateral bedforms. Its occurrence above carbonate and fine-grained deposits indicates a shift toward higher energy flow conditions and enhanced sediment supply within the depositional system.

 doi:10.20944/preprints202602.0078.v1

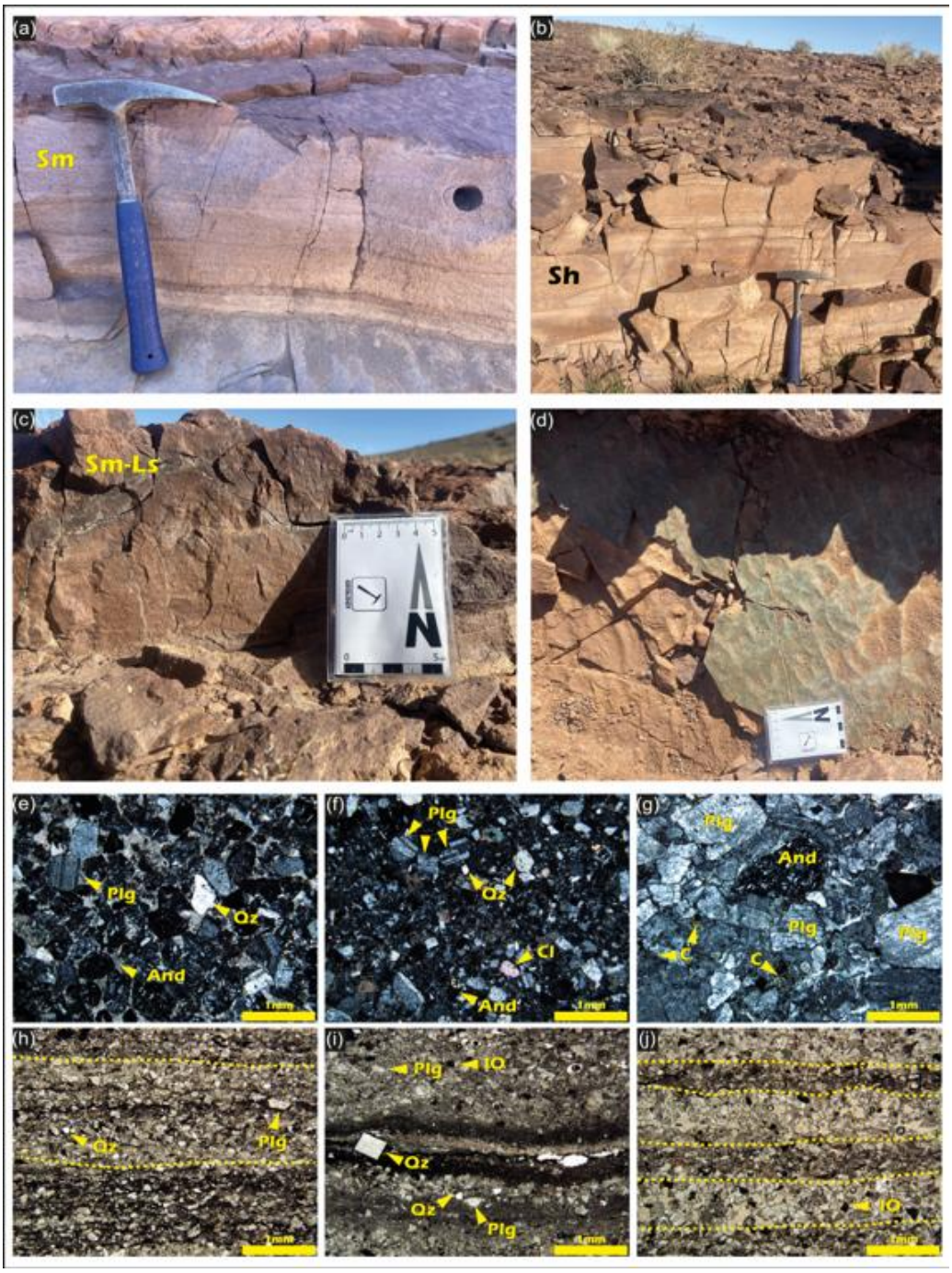

Figure. 5. Field and microscopic photographs of sandstone facies; (a) Massive sandstone (Sm) showing poorly defined laminations; (b) Horizontally bedded sandstone (Sh); (c) Massive sandstone (Sm) with stromatolitic lamina; (d) Ripple marks observed at the top of sandstone beds; (e) - (f) Photomicrographs in crossed polarized light of facies Sm from the Amane n'Tourhart area; (g) Photomicrograph in crossed polarized light showing facies Sm of arkosic sandstone from the Tifernine area; (h) – (i) Photomicrographs in crossed polarized light of facies Sh from the Amane n'Tourhart area (And: Andesite; Qz: Quartz; Plg: Plagioclase; Cl: Calcite; PC: Clay; IO: Iron Oxide).

F5: Horizontally bedded sandstone (Sh)

Description: This facies is absent in the Tifernine area, but occurs in Amane n'Tourhart (Figure 2) as horizontally stratified, lenticular to tabular beds of medium- to coarse-grained reddish sandstones. Laminae are at millimeter scale, flat to slightly wavy, parallel, and generally horizontal, with flow directions varying locally (e.g., N10 in AT01, N160–N35 in AT03). The facies commonly grades to

 doi:10.20944/preprints202602.0078.v1

stromatolitic (Ls1) or conglomeratic (Gmm, first type peperite) facies. Microscopically, lighter laminae are rich in detrital grains (quartz, plagioclase, altered andesite) with minimal cement or matrix, while darker laminae are cement- and matrix-rich, composed of ferruginous carbonate micrite or clay. Opaque minerals, mainly iron oxides, are ubiquitous, and microbial mat textures are preserved (Figures 5 (d) and (f)).

Interpretation: The horizontally laminated sandstones are interpreted as traction-dominated deposits formed under upper-flow regime conditions in shallow channels or on flood plains during episodic high-energy flows. The planar laminae reflect laminar to minimally turbulent transport of medium- to coarse-grained sediment, while alternating grain-rich and matrix-rich laminae indicate fluctuations in flow competence and sediment supply [72].

F6: Massive siltstone-mudstone (Fm2)

Description: This facies has a non-erosive, flat base and consists of friable, mud-rich siltstones that are highly susceptible to erosion. It ranges in thickness from 0.15 to 4 m (Figures 2, 5 (e)). It underlies and is associated with the massive sandstone facies, but always occurs below the muddy siltstone facies with limestone nodules (Fm1) (Figures 2, 5 (e)).

Interpretation: The deposition of this facies, characterized by a non-erosive base and representing the upper part of normally graded fluvial deposits, indicates the accumulation of fine-grained sedimentary material transported in suspension by muddy flows during flood events [73,74].

4.1.2. Carbonate facies

F7: Massive limestone (Lm)

Description: In the Amane n'Tourhart area (Figure 2), this facies is lenticular to tabular with an erosive base, up to 1m thick, and is whitish to yellowish in color. It is always above Ln facies (nodular limestone) or facies Fm1 (muddy siltstone with limestone nodules). At their transition zone, carbonate material becomes more abundant than detrital material, nodules progressively evolve from solitary to coalescing, and the detrital material disappears in case of muddy siltstone. In places, especially towards the top, stromatolitic structures are apparent (Figure 6 (d)). Limestone consists of either grains, forming grainstone, or contains stromatolites, forming bindstone. Thin-section analysis of this facies reveals that it is composed predominantly of sparite and, locally, microsparite, and lacks micrite (Figures 10 (d) and (e)). Large spherulitic structures are notably observed, ranging from 5 mm to 1 cm in diameter. Calcite is partially replaced by silica (Figure 10 (d)). This facies is absent at the Tifernine area.

Interpretation: The upward transition from muddy siltstone with carbonate nodules (Fm1) through nodular limestones (Ln) to massive limestones (Lm) reflects a gradual increase in carbonate deposition and a progressive reduction in detrital input. This stratigraphic trend records a shift from a shallow-water, fluvially influenced depositional setting toward a more stable, low-energy lacustrine environment dominated by chemical sedimentation. Across these facies (Fm1–Ln–Lm), carbonate spheroids are commonly observed. Spherulite growth is favored by high levels of Mg and silica in highly alkaline solutions, resulting in rapid calcite crystal growth, with or without any microbial influence [75–77]. These spheroidal or spherulitic features are interpreted as chemical precipitates formed in supersaturated, quiescent lacustrine waters, reflecting episodes of limited clastic supply and increased carbonate saturation [78–80]. Their development throughout the transition indicates progressive stabilization of the depositional system and enhanced chemical precipitation in the basin under semi-closed hydrological conditions [81].

F8: Nodular limestone (Ln)

Description: This facies occurs only in the Amane n'Tourhart area. It is lenticular to tabular in shape, has an erosional base, and ranges from 0.25 to 1.25 m in thickness (Figure 2). It forms the transition zone between the Fm1 facies (muddy siltstone with carbonate nodules) and the massive

 doi:10.20944/preprints202602.0078.v1

limestone facies (Lm); its color is variegated with white nodules and red siltstone (Figure 6. (a)-(c)); and it is calcareous when carbonate nodules are abundant (as is the case for AT02) (Figures 2 (b), 6 (c)). This facies includes rudstone, formed during periods with high-energy water conditions. The nodules are commonly irregular to spheroidal in shape and display concentric and radial internal microfabrics. Under the microscope, this facies displays two distinct components: red, detrital material-rich and white, micritic laminae. White to yellow nodular parts consist of micritic to microsparitic calcite, with some contribution of detrital components (Figure 6 (b)), showing spherulitic (Figure 6 (c)) or microstromatolitic textures. Red, siltstone laminae comprise quartz and altered plagioclase grains within a micritic matrix.

Interpretation: Presence of both stromatolitic and micritic to microsparitic nodules suggests that carbonate precipitation occurred through a combination of physicochemical and microbial processes [81,82]. Such stromatolitic–nodular associations correspond to the "mobile buildups" described by [83], which develop in very shallow lacustrine to palustrine settings where carbonate forms within soft, weakly lithified sediments. These buildups remain unstable and may be displaced, deformed, or partially reworked by low-energy currents or water-level fluctuations, resulting in irregular stromatolitic lamination and nodular carbonate textures. In this setting, carbonate precipitation was mainly driven by CO_2 degassing, evaporation, and increased alkalinity of pore waters, while microbial films acted as nucleation centers for localized carbonate precipitation [84]. Presence of detrital grains indicates a siliciclastic input from an adjacent floodplain, consistent with deposition along the margin of a shallow, low-energy lake [79]. Overall, the Ln facies represents the onset of lacustrine carbonate sedimentation, marking the transition from fluvial sedimentation (Fm1) to chemical, carbonate precipitation (Lm) [20] . It reflects a shallow lacustrine–palustrine environment characterized by fluctuating hydrological conditions, periodic exposure, and early diagenetic cementation leading to the development of nodular textures [85,86]. This facies thus records progressive establishment of lacustrine conditions in a predominantly continental depositional system.

 doi:10.20944/preprints202602.0078.v1

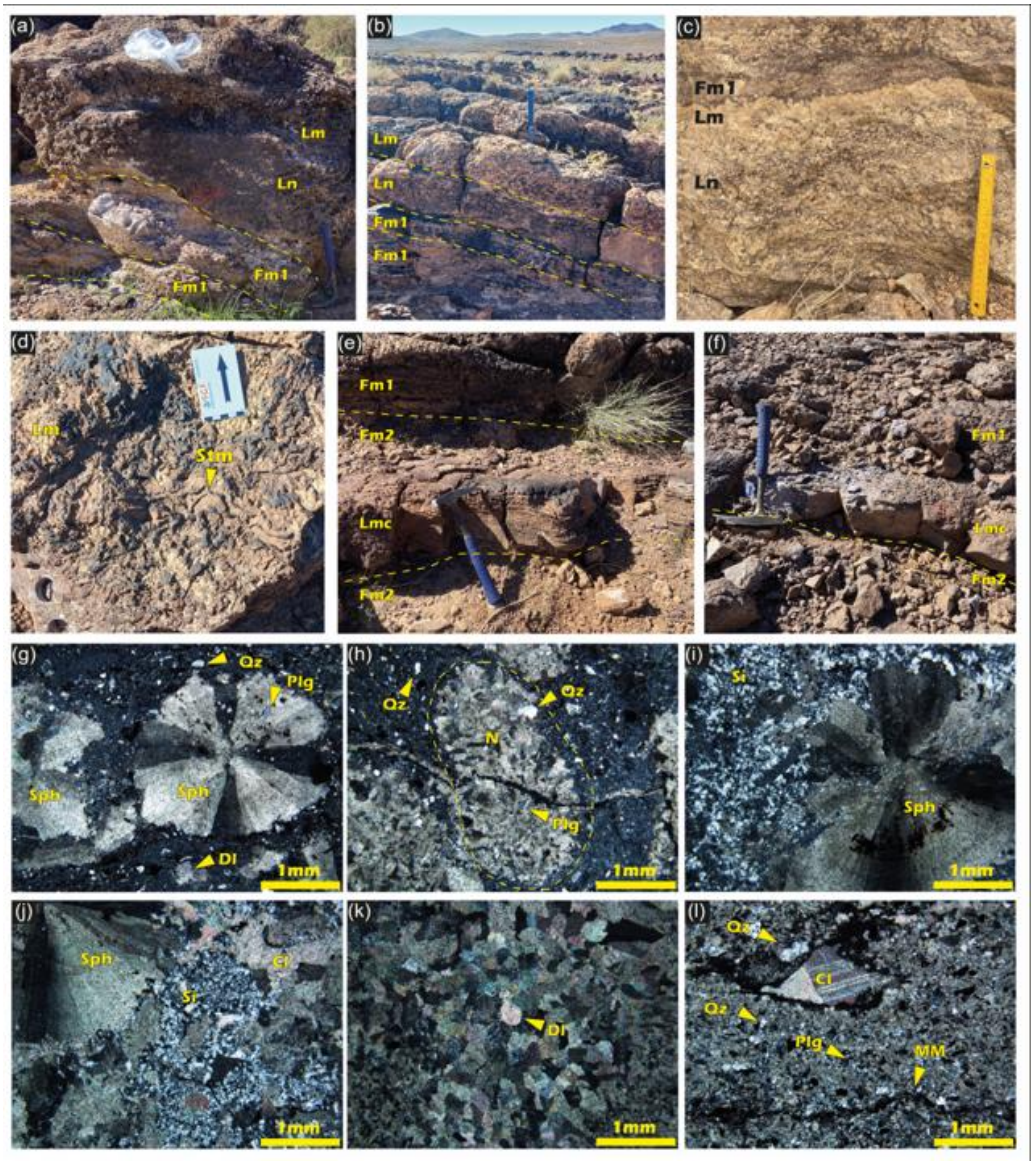

Figure. 6. Field and microscopic photographs of different facies (Fm1, Ln, Lm, and Lmc) from the Amane n'Tourhart area; (a) Erosional base of massive siltstone-mudstone facies with carbonate nodules (Fm1), nodular limestone (Ln), and massive limestone (Lm); (b) Erosional base of facies Fm1, Ln, and Lm showing a tabular geometry; (c) The cross-sectional view highlights the distinction between facies Fm1, Ln, and Lm; (d) Stromatolitic buildup at the top of facies Lm; (e) - (f) Massive limestone with scattered clasts (Lmc) displaying tabular and lenticular shapes; (g) Photomicrograph of facies Fm1, showing spheroidal nodules of spherulites; (h) – (i) Photomicrographs of facies Ln., (j) – (k) Photomicrographs of facies Lm. L. Photomicrograph of facies Lmc. (Qz: Quartz; Plg: Plagioclase; Dl: Dolomite; Cl: Calcite; Si: Silica; Sph: Sphalerite; MM: Microbial Mat; N: Nodule).

F9: Laminar Limestone (Ll)

Description: This facies is typical for the Tifernine area, occurring in tabular to lenticular beds, 0.5–4 m thick (Figure 3), composed of horizontal to locally inclined pelitic laminae at centimeter- to millimeter-scale, and with occasional sandstone beds. The laminae display mud cracks, micro-ripples, cross-bedding, and E-W-oriented ripple marks (N110) (Figure 7). Some beds show soft-sediment deformation and are brecciated, forming the Lli facies. Microscopically, basal layers show micritic and microsparitic laminae of calcite, sandy laminae with quartz, plagioclase, and andesitic fragments in a ferruginous matrix, and pelitic seams with EPS, microbially induced sedimentary structures (MISS), and iron oxides (Figure 8). In the middle part, sandy laminae and pelitic seams are

 doi:10.20944/preprints202602.0078.v1

rare, while micritic and microsparitic calcite and micrometer-scale extracellular polymeric substances (EPS) structures are more pronounced. The upper part resembles the basal beds, with microsparite and reappearance of thin, sandy laminae or sandstone beds containing altered quartz and plagioclase.

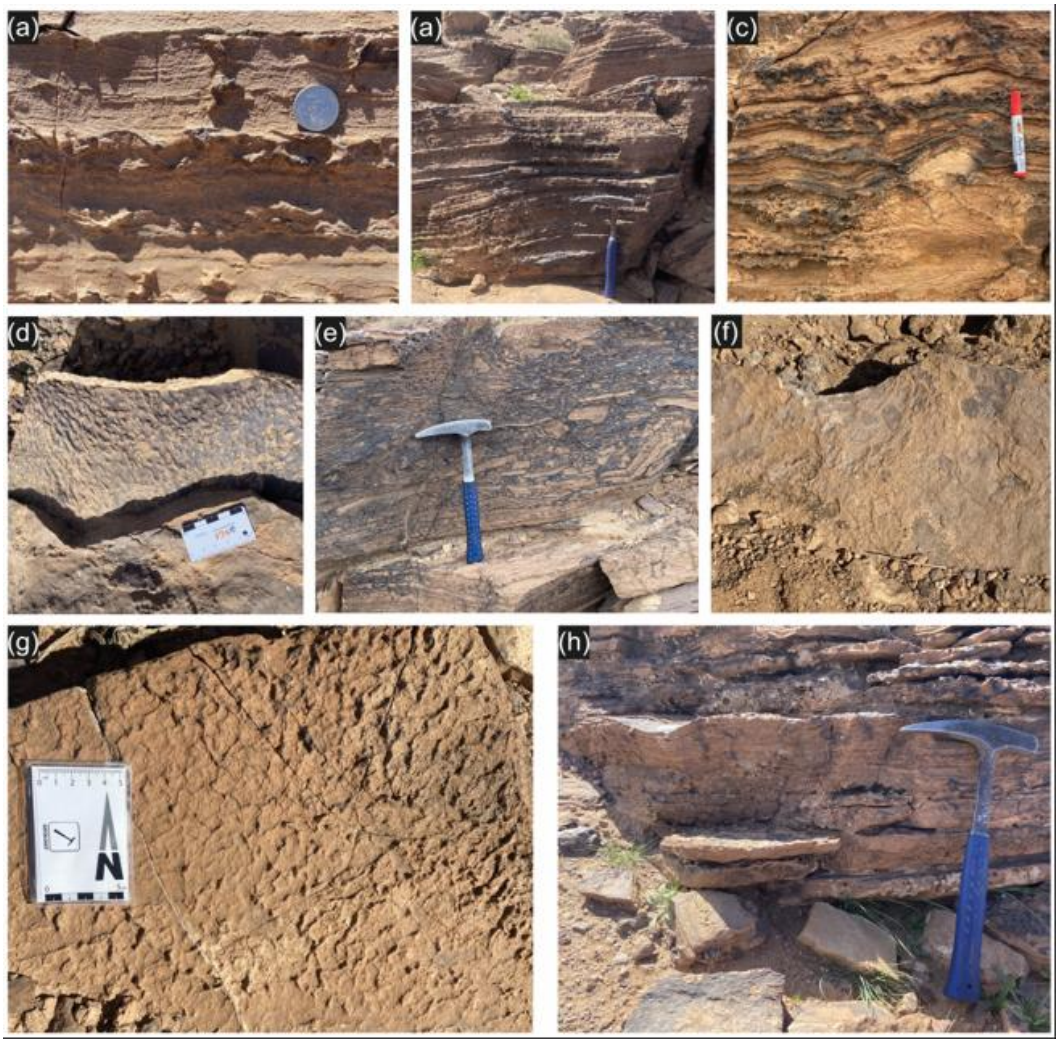

Figure 7. Field photographs of carbonate limestone facies (Ll) from the Tifernine area.; (a) Irregular lamination in carbonates with pelitic seams; (b) Laminated limestone facies (Ll) showing large undulations at the base of the bed; (c) Laminated limestone (Ll) with asymmetric ripple marks; (d) Micro-ripples organized in an "elephant-skin", representing microbial structures (MISS: Microbially Induced Sedimentary Structures); (e) Intraclastic, laminated limestone facies (Lli); (f) Flat-pebble conglomerate at the top of the laminated limestone facies; (g) Tuffeted microbial structure developed at the top of the laminated limestone bed; (h) Symmetrical ripples observed within the laminated limestone (Ll).

 doi:10.20944/preprints202602.0078.v1

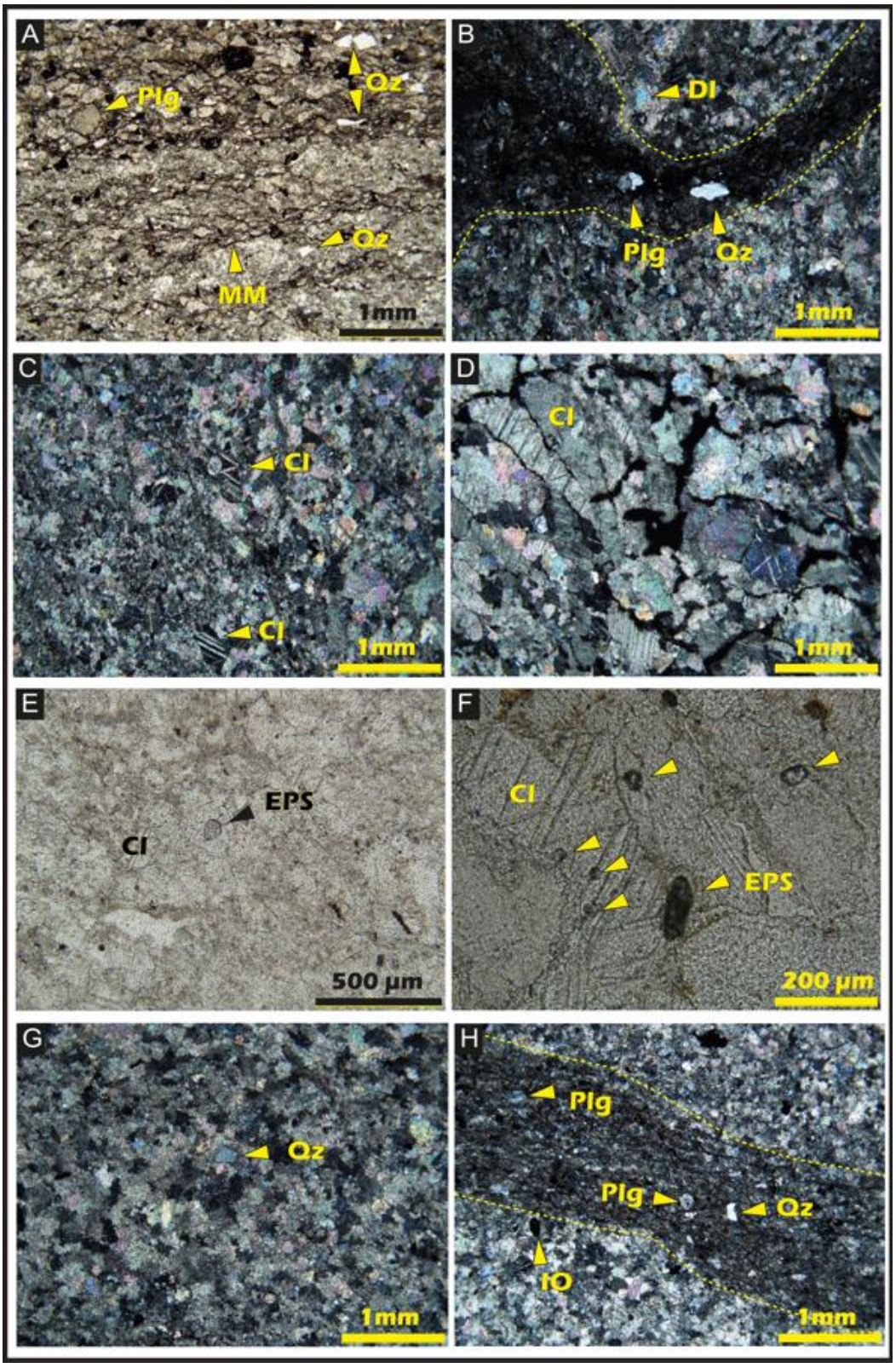

Figure 8. Photomicrographs showing the carbonate limestone facies (Ll) from the Tifernine area; (a) Photomicrograph in cross-polarized light from the lower part of the unit, rich in detrital clasts and microbial mats; (b) – (c) Photomicrographs in cross-polarized light showing pelitic laminae (B) and microsparitic calcite (C); (d) Photomicrograph in cross-polarized light from the middle part of the unit showing calcite crystals associated with iron oxides; (e) – (f) Photomicrographs in polarized light under high magnification of facies Ll showing Extracellular Polymeric Substances (EPS); (g) – (h) Photomicrographs in cross-polarized light from the upper part of the unit showing microsparitic calcite (G) and a sandstone lamina (H) (Qz : Quartz; Cl : Calcite; Plg : Plagioclase; MM : Microbial Mats; IO : Iron Oxide).

 doi:10.20944/preprints202602.0078.v1

Interpretation: Grainstones of this facies, together with mud cracks, ripple marks, laminae, and pelitic seams, indicate deposition in a shallow, freshwater lacustrine environment that was generally calm, but experienced episodic high-energy events and emersion [84,87,88]. The laminae contain microbial structures, such as tuffeted microbial mats and MISS, along with iron oxides and small EPS, rounded to elongated ([89–95]. These features suggest that microbial activity played a significant role in sediment stabilization, promoting localized carbonate precipitation and contributing to the formation of laminated fabrics. The coexistence of detrital grains with micritic carbonate reflects a mixed origin, where carbonate accumulation was controlled by both physicochemical processes, such as CO_2 degassing, evaporation, and increased alkalinity of interstitial waters, and by microbial mediation at low-energy, intermittently exposed lacustrine margin [81,82,84]. Overall, this facies records a dynamic, shallow-lacustrine system characterized by episodic flooding, periodic exposure, microbial colonization, and early diagenetic cementation, reflecting progressive establishment of lacustrine conditions within a dominantly continental depositional framework.

4.1.3. Mixed facies

F10: Massive siltstone-mudstone with carbonate nodules (Fm1)

Description: This facies is characterized by a tabular and sometimes laterally discontinuous (lenticular) shape, with an erosive base, and varies in thickness from 30 cm to 3.5 m (Figures 2, 6 (a) – (f)). This facies always underlies the Ln facies (nodular limestone) and it underlies / is associated with the Lmc facies (massive limestone with scattered clasts). It is composed of red and purple, clay-rich siltstone with white carbonate nodules (Figure 6 (c)). These nodules are solitary and frequently spherulitic. Microscopically, this facies resembles the nodular limestone facies, displaying two distinct components. The reddish, clay-rich siltstone component contains fine-grained quartz and plagioclase within micritic matrix (Figure6 (a)). The nodular component is less abundant in this facies (Fm1) compared to Ln facies. The nodules consist of microsparitic to sparitic calcite and contain spherulitic structures that are smaller in size than those observed in Ln and Lm facies (Figure 6. (a)).

Interpretation: Fm1 represents deposition in shallow, low- to moderate-energy fluvial channels, where episodic, ephemeral flows transported mud and silt and allowed localized carbonate precipitation along intermittently exposed margins [64,96]. Evaporation and elevated alkalinity during early diagenesis, promoted formation of small spherulitic calcite nodules, while input of fine-grained quartz and plagioclase reflects proximal siliciclastic sources [81,82,84]. This facies marks the initial phase of carbonate precipitation in a fluvial-lacustrine transitional setting, preceding more extensive nodular and massive carbonate deposition.

F11: Massive limestone with scattered clasts (Lmc)

Description: This red to purple, pebbly massive limestone facies occurs as lenticular beds 0.2 to 0.35 m thick and extent laterally for meters (Figures 2, 6 (e) and 6 (f)). Generally, it is massive with poorly defined laminae (sometimes planar) and contains clasts. Microscopic observations reveal that the facies consists of grainstone, with calcite crystals set within a micritic and/or microsparitic matrix, containing abundant quartz and altered plagioclase grains. Iron oxide minerals and microbial mats are abundant throughout this facies (Figure 6 (f)).

Interpretation: This clastic limestone facies, characterized by basal laminations and a notable presence of detrital quartz, was deposited in a relatively deep and tranquil lacustrine environment. The grainstone textures and the abundance of detrital quartz indicate transport and deposition under non-negligible hydrodynamic energy, as such grains require traction or suspension processes capable of overcoming settling in low-energy conditions.. Gradual rise in the lithoclast content towards the top of the facies suggests an increase in depositional energy, likely due to either a decrease in water level or turbidity currents transporting clastic material to the deeper parts of the lake [63,79,88].

F12: Stromatolitic limestone (Ls)

 doi:10.20944/preprints202602.0078.v1

Description: Stromatolitic beds are abundant in the Amane n'Tourhart area, but absent in Tifernine, occurring mainly at the top of the lacustrine sequence (Figure 2). Following Freytet and Verrecchia [83]. three types can be distinguished based on morphology. Ls1, the inclined columnar stromatolites (Figure 9 (a) – (d)), form thick bioherms up to 5 m, with small- to medium-size domal columns, oriented NW–SE to E–W parallel to paleocurrents (Figure 14 (a)). Laminae alternate between red, detrital and white, carbonate components. This facies is sometimes interlayered with Lm or Fm1 facies, and could be partially silicified. Ls2, domal stromatolites, develop on the Ls1 facies, forming vertical, attached or isolated domes up to 2 m in size (Figure 9 (e) – (g)), with laminae alternating between detrital and carbonate components, frequently replaced by silica. Ls3, stratiform stromatolites, represent the uppermost stromatolitic deposits before stromatolite disappearance, forming planar laminae or small isolated domes up to 30 cm in size (Figure 9 (h)), with alternations of red, detrital and pale, calcareous or siliceous components. Laminations could be continuous or discontinuous, locally displaying soft-sediment deformation similar to seismites (Figure 9 (i)). Microscopically, red laminae are composed of quartz grains embedded in a ferruginous cement, whereas white laminae consist of micritic to sparitic calcite occasionally containing spherulites and synsedimentary micro-deformation structures within beds (Figures 10 (a) – (d)). Partial preservation of EPS and ferruginous, irregularly laminated microbial mats (Figures 10 (f) – (h)) suggests microbial mediation during early diagenesis, while locally developed silicification (Figure 10 (e)) suggests early diagenetic replacement under silica-rich pore-water conditions.

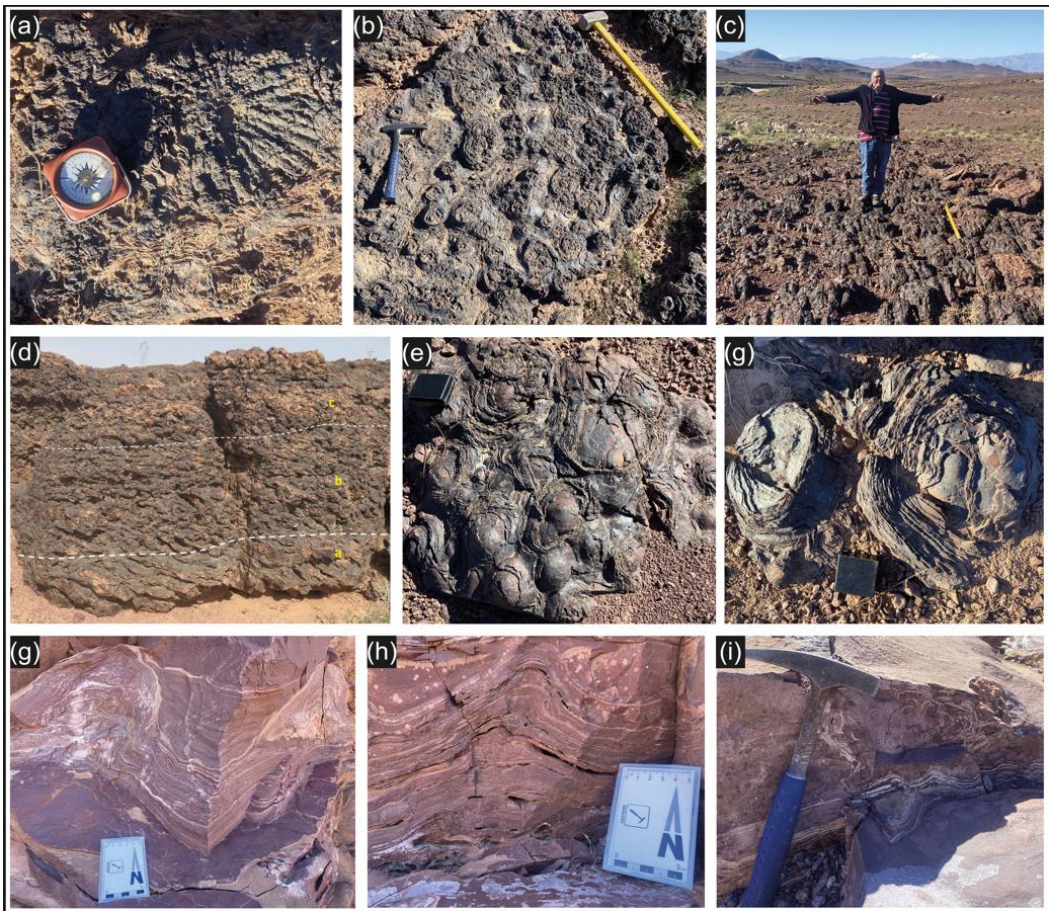

Figure. 9. Field photographs of stromatolitic limestone facies (Ls) from the Amane n'Tourhart area; (a) An isolated stromatolite; (b) Bedding-plane view of inclined Ls1 facies with small-sized structures; (c) Inclined, columnar Ls1 facies; (d) A block of Ls1 showing the evolution in columnar stromatolites: at the base stratiform "**a**", in the middle inclined "**b**", and at the top subvertical "**c**"; (e) – (g) Dome-shaped Ls2 facies. (h) Small, isolated dome-shaped Ls3 facies. (i) Ls3 facies with seismite showing disorganized lamination.

 doi:10.20944/preprints202602.0078.v1

Interpretation: The stromatolite facies Ls1–Ls3 represent a progressive evolution in microbial carbonate accumulation in shallow-water, lacustrine environments with variable hydrodynamics. The Ls1 facies inclined columnar stromatolites developed in fast-flowing, turbulent conditions, associated with a slope break along riverbeds, weirs, small rapids, or minor waterfalls, where microbial mats, including EPS, could grow on a sloped substrate while recording paleocurrent directions [81]. Alternating red, detrital and white, carbonate laminae reflect episodic siliciclastic input and carbonate precipitation. The Ls2 facies domal stromatolites formed in a slower flowing, laminar zone, such as a protected riverbed area or a palustrine setting, often on a microtopographic high. These facies laminae are frequently affected by silicification with EPS preserved, indicating microbial mediation [79,96]. The Ls3 facies stratiform stromatolites, the stratigraphically highest microbial carbonate deposits, occur in thin beds (≤30 cm thick) as planar laminae or small domes, composed of red, detrital and white, marly or siliceous components with rare, carbonate-poor component. Soft-sediment deformation and seismite structures record episodic lake-bottom disturbance. Taken together, these facies record the onset, development, and eventual decline of stromatolitic growth under fluctuating hydrodynamic, sedimentary, and geochemical conditions, marking the transition from active microbial carbonate precipitation to non-carbonate, lacustrine deposition [82,84].

 doi:10.20944/preprints202602.0078.v1

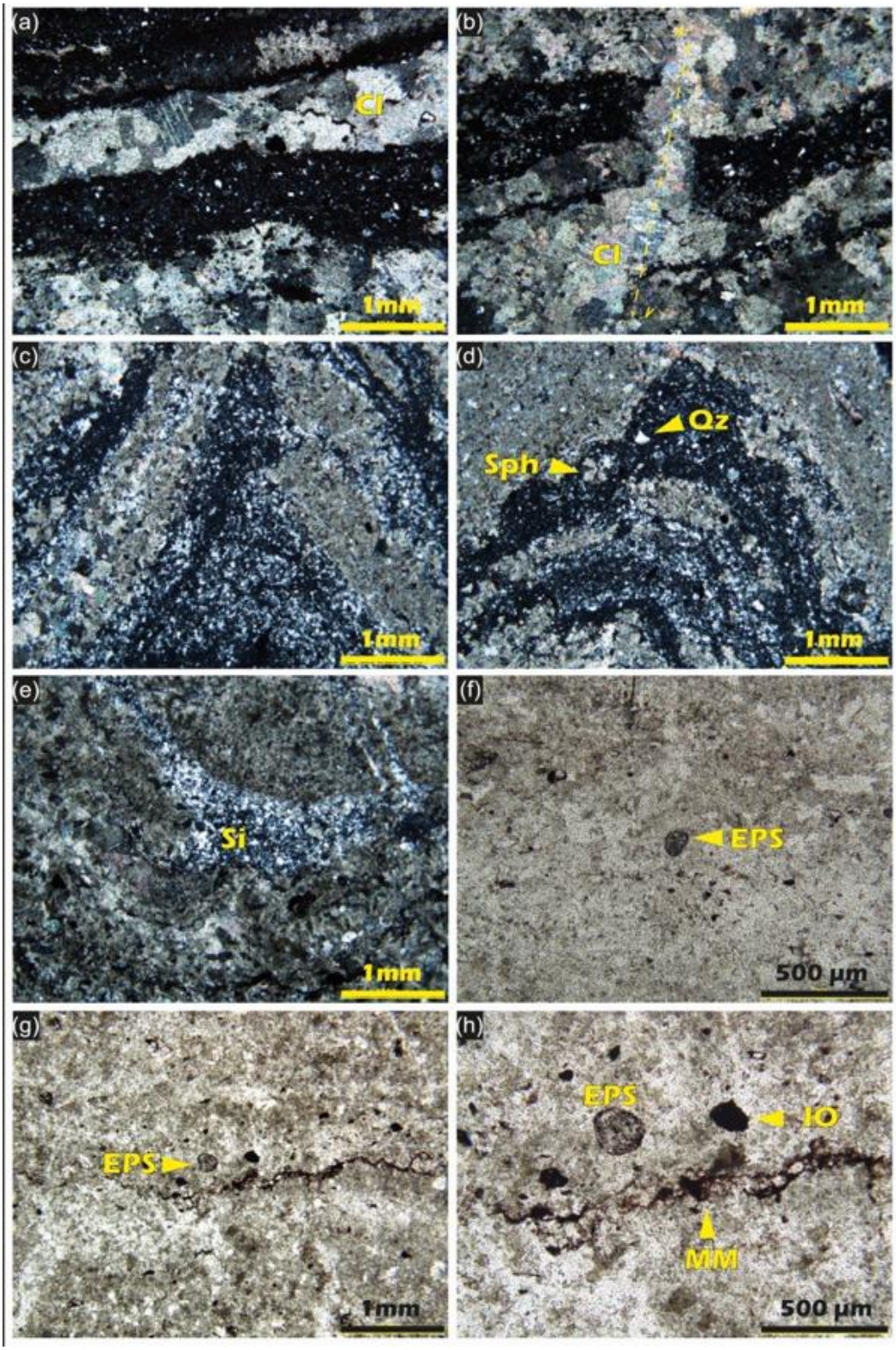

Figure 10. Photomicrographs showing microstructural features of stromatolitic limestone facies (Ls1 and Ls2) from the Amane n'Tourhart area; (a) – (b) Photomicrographs under crossed polarized light of the Ls2 facies showing alternating dark, siliciclastic and light, carbonate laminae, with synsedimentary micro-deformation textures and a small, normal micro-fault within a siliciclastic lamina; (c) – (d) Conical and columnar stromatolites in the Ls1 facies displaying spherulitic textures within the siliciclastic laminae. (e) Partial dissolution of the Ls facies and silica replacement; (f) – (h) Photomicrographs under crossed polarized light showing Extracellular Polymeric Substances (EPS) and Microbial Mats (MM). (Qz: Quartz; Cl: Calcite; Si: Silica; Sph: Spherulite; IO: Iron Oxide).

 doi:10.20944/preprints202602.0078.v1

4.1.3. Volcanic facies

In the Amane n'Tourhart area, fluviolacustrine deposits lie unconformably on an andesitic-dacitic substratum (Figure 11 (a)). Brecciated andesites (Figure 11 (b)) occur at the top and contain lithic clasts within an andesitic lava. These andesites also exhibit Neptunian dikes infilled with sediments younger than the lava, occupying open fractures. A dyke emplaced after the basin development cuts across both the sedimentary and volcanic units (Figure 11 (c)). Both types of lava (andesites and breccia andesites) are associated with the post-caldera stage and represent the youngest volcanic units in the Oued Dar'a Caldera (ODC) succession [40]. The porphyritic andesites at the base of the formation contain crystals of plagioclase and pyroxene, both of which are altered and embedded within a microlitic groundmass (Figure 11 (a)). The brecciated andesites at the top of the formation are characterized by phenocrysts of pyroxene (clinopyroxene and orthopyroxene) and altered plagioclase, together with plagioclase microlites and quartz clasts (Figure 12 (b)).

In the Tifernine area, the carbonate deposits are underlain by microlitic andesites and overlain by brecciated rhyolites (Figure11 (d)). Microscopically, the andesites at the base of the carbonate formation are altered and display a microlitic texture with a few rare plagioclase phenocrysts smaller than 1 mm (Figure 12 (c)). In contrast, the rhyolite at the top of the formation shows a porphyritic texture characterized by strongly altered plagioclase phenocrysts and quartz crystals, with plagioclase microlites embedded in a glassy matrix (Figure 12 (d)).

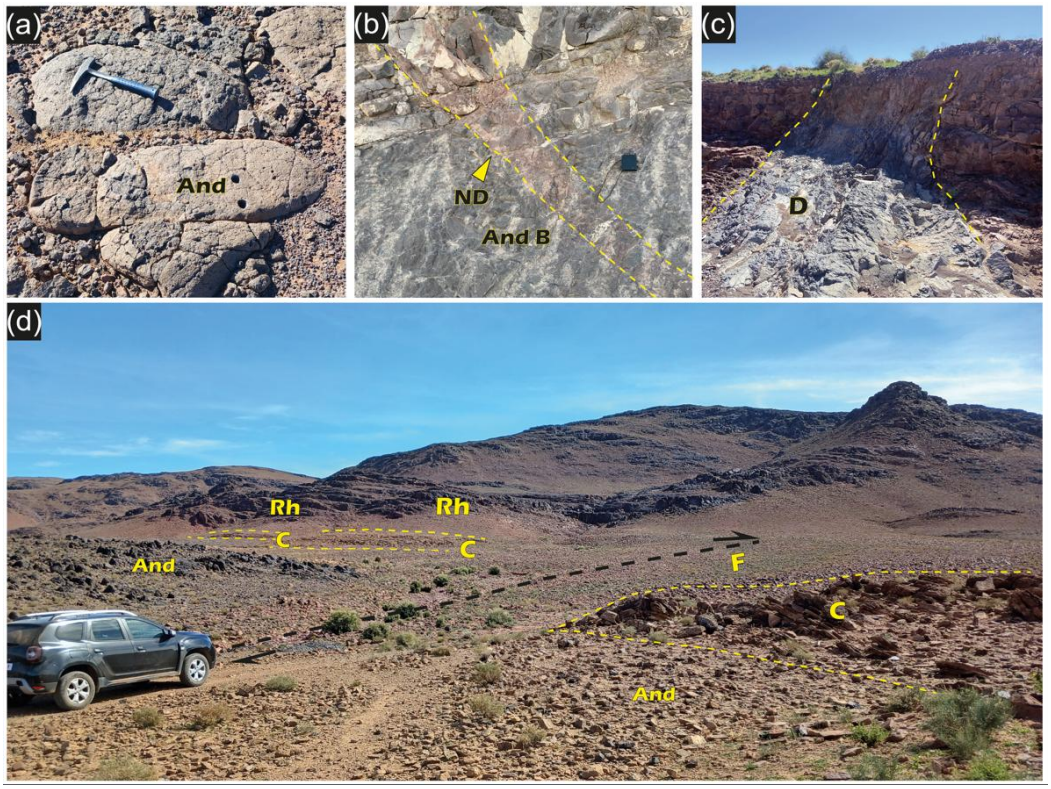

Figure 11. Field photographs showing volcanic facies from the Amane n'Tourhart and Tifernine areas; (a) Andesitic lava from the Amane n'Tourhart area; (b) Andesitic breccia overlying the fluviolacustrine deposits of the Amane n'Tourhart area, crosscut by a Neptunian dike; (c) Dyke cuts the fluviolacustrine unit in the Amane n'Tourhart area; (d) Panoramic view of the Tifernine area showing the Tifernine lacustrine unit underlain by andesites and overlain by rhyolites, with the carbonate unit offset by a dextral fault (And: Andesite; And B: Andesitic Breccia; ND: Neptunian Dike; D: Dyke; C: Carbonate; Rh: Rhyolite; F: Fault).

 doi:10.20944/preprints202602.0078.v1

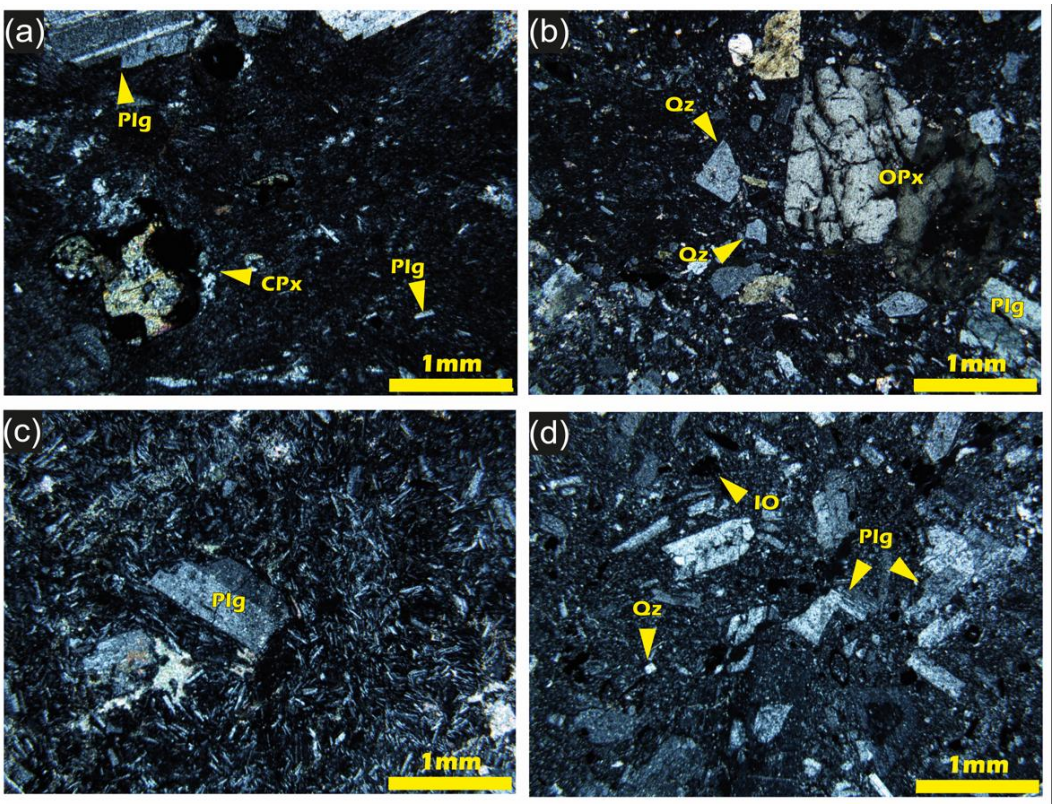

Figure 12. Microscopic photographs of volcanic facies; (a) Porphyritic andesite in the Amane n'Tourhart area; (b) Brecciated andesite in the Amane n'Tourhart area; (c) Microlitic andesite in the Tifernine area; (d) Rhyolite in the Tifernine area. (Qz: Quartz; Plg: Plagioclase; And: Andesite; CPx: Clinopyroxene; OPx: Orthopyroxene, IO: Iron Oxide).

4.1.4. Biogenic features of the Stromatolitic limestone (Ls) facies in Amane n'Tourhart and the Laminar limestone (Ll) facies in Tifernine

Biological processes played a fundamental role in the development of the laminated structures. Scanning Electron Microscope (SEM) observations reveal three populations of micrometric structures distinguished by recurring morphologies, size ranges, spatial distribution, and consistent association with stromatolitic lamination (Figure 13). Their repeated occurrence, organization parallel to laminae, and close relationship with micritic carbonate precipitates support a biogenic origin according to widely accepted criteria for Precambrian biosignatures [81,82,94]. On this basis, these structures are interpreted as fossilized microbial remains rather than abiotic precipitates.

The observed components include calcified micritic aggregates, calcified filamentous organic structures, and micrometric spheroidal to tubular bodies interpreted as bacterial-like microbial remains. These occur exclusively within laminated facies, notably stromatolites (Ls) and laminated limestones (Ll) (Figure 13). Calcified micritic aggregates occur as irregular to elongated or locally subcircular forms, approximately 300 μm in length and 10–15 μm in width. Calcified filamentous structures are elongated elements displaying tubular, irregular morphologies with rough terminations (Figure 13 (d) –(f) – (k)). These filaments are locally curved and occasionally tapered. Their walls, measuring a few micrometres in thickness and up to 5–10 μm in diameter, are composed of calcite (Figure 13 (i)), consistent with early mineralization of organic templates [97]. These filamentous structures are preferentially preserved within intergranular and fenestral spaces of the lithified sediments, where early cementation favored their stabilization. Their morphology, size range, and spatial organization are comparable to filamentous microbial remains reported from ancient lacustrine and peritidal carbonates, and they are therefore interpreted as fossilized microbial filaments, without implying precise taxonomic affinity [20,98].

 doi:10.20944/preprints202602.0078.v1

Micrometric plate-like to tubular substances, interpreted as fossilized extracellular polymeric substances (EPS), occur either as isolated bodies (Figure 13 (g) – (i) – (l)) or in close association with filamentous structures (Figure 13 (d) – €). These features range from ~20 to 60 µm and consistently adhere to detrital grains or calcite crystals, reflecting their role in trapping, binding, and mineral nucleation during early diagenesis. In ancient systems, such EPS-like fabrics are widely regarded as robust indicators of microbial activity, even in the absence of molecular biomarkers [82,94,99].

Although direct identification of specific microbial taxa is not possible, the convergence of morphological, sedimentological, and petrographic evidence strongly supports the presence of an active microbial consortium influencing carbonate precipitation and lamination development during deposition. This interpretation is further supported by lipid biomarker evidence from the Amane n'Tourhart stromatolites reported by Carrizo et al. [27], which documents the presence of bacterial-derived compounds, confirming active microbial communities during carbonate deposition. In addition, the microbial textures and carbonate–microbe interactions identified here closely resemble those described by Chraiki et al. [24] in coeval Ediacaran carbonate systems. Together, these independent petrographic and geochemical datasets provide convergent evidence for a significant bacterial contribution to carbonate precipitation and lamination development in these Ediacaran lacustrine environments.

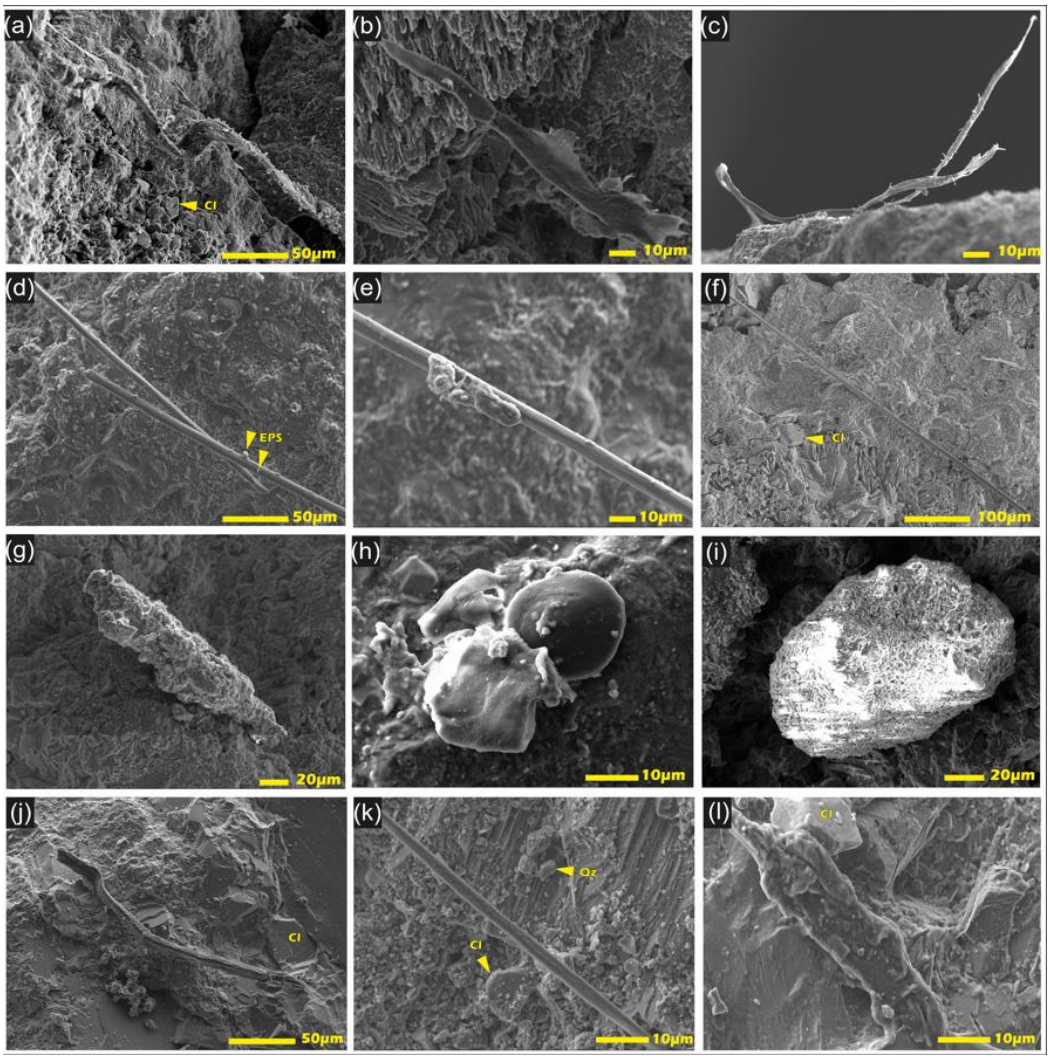

Figure 13. Scanning Electron Microscope images showing the biogenic features in stromatolitic limestone (Ls1) and (Ls2) and laminar limestone (Ll); (a) – (c) Elongated calcified structures in (Ls1) and (Ls2); (d) – (e) Calcified organic filaments and EPS in Ls1; (f) Calcified organic filaments in Ls2; (g) – (i) EPS attached to detrital grains in Ls1 and Ls2; (j) Elongated calcified structure in Ll; (k) Calcified organic filaments in Ll; (l) EPS attached to calcite crystals in Ll. (Qz: Quartz; Cl: Calcite).

 doi:10.20944/preprints202602.0078.v1

4.2. Facies Associations

In the study areas, the sedimentary facies are stratigraphically organized into sequences or facies associations, which record the sedimentary processes occurring within their depositional environment. These facies associations reflect the vertical and lateral arrangement of deposits formed in laterally adjacent sub-environments. The stratigraphic arrangement was controlled by cyclicity driven by water-level fluctuations, channel migration, lake filling, progradation and retrogradation of the alluvial-fluvial system, and the expansion or shrinkage of the lacustrine system.

- **Amane n'Tourhart area**

a) Alluvial fan facies association

This facies association is made up of a succession of conglomerates (Gcm, Gmm, and Gt), sandstones (Sm and Sh) and clay-bearing siltstones (Fm1 and Fm2). It reflects periods of incision of river channels, followed by phases of filling during floods with high sediment and fluid flows, and finally periods of decreased water energy in the aftermath of floods [72,100,101]. This facies association is characteristic of alluvial fan deposits. Dominated by coarse, reddish-purple clastic material, it represents a braided-type fluvial system, located in the proximal and medial parts of the alluvial fans. The conglomerates and sandstones correspond to debris-dominated flows deposited in channels and bars [64,102]. Abandonment or migration of the channels allowed deposition of massive siltstone-mudstone beds with calcareous nodules, corresponding to a low-energy floodplain environment.

b) Lake facies association

This facies association records a progressive transition from fluvial to lacustrine environments within the studied basin. It begins with clay-bearing siltstones containing limestone nodules (Fm1), which indicate deposition under low-energy fluvial conditions dominated by fine-grained sediment settling in overbank or shallow floodplain settings associated with ephemeral channels [100]. The carbonate nodules are interpreted as early diagenetic features, formed within the sediment through localized carbonate precipitation during periods of reduced sedimentation and enhanced pore-water saturation, rather than as primary lacustrine carbonate deposits. Their development reflects intermittent water ponding and fluctuating hydrological conditions, which promoted carbonate supersaturation in pore waters and nodule growth during early burial. Although Chraiki et al. [24] originally interpreted Fm1, Ln, and Lm as thrombolitic facies, carbonates of these facies do not represent thrombolites, but are interpreted here as early diagenetic nodules.

The Fm1 facies is succeeded by nodular limestones (Ln), marking a transitional zone between fluvial and shallow-water, lacustrine conditions. The nodules, including micritic, microsparitic, and stromatolitic components, reflects early diagenetic carbonate precipitation in a shallow-water, low-energy lake environment, where microbial mats locally contributed to carbonate nucleation. Detrital grains, including quartz and plagioclase, indicate a siliciclastic input from nearby floodplains, while the presence of small stromatolites suggests limited microbial activity under fluctuating hydrological conditions [81,82]. The sequence culminates with massive limestones (Lm), representing deposition in a more persistent, deeper-water, lacustrine setting, where carbonate precipitation was largely chemical, under relatively stable water-column conditions [88,103]. The transition from Fm1 through Ln to Lm thus captures a gradual shift from predominantly siliciclastic, fluvial deposition to carbonate-dominated, lacustrine sedimentation, highlighting variations in water depth, hydrology, and sediment supply across the lake basin.

- **Tifernine area**

Lacustrine facies association

The siltstone-mudstone facies (Fm2) with laminar limestone (Ll) represents deposition in calm, low-energy offshore zone of the lake [79]. The fine-grained sediments settled from suspension in quiet water, resulting in the formation of thin, laterally continuous laminae of microsparitic to sparitic limestone, interbedded with claystone and sandstone laminae in the lower and upper parts of the Tifernine Formation. This facies reflects periods of relatively stable water-level and minimal siliciclastic input, in contrast to the more proximal, higher-energy fluvial or shallow-water, lacustrine

 doi:10.20944/preprints202602.0078.v1

facies (Fm1 and Ln) present elsewhere in the basin. Overall, Fm2 and Ll record quiet, offshore sedimentation in a stratified lacustrine environment, preserving fine-scale, primary sedimentary structures and subtle microbial and early diagenetic features.

5. Discussion

5.1. Paleo-Environmental Reconstruction of the Amane n'Tourhart and Tifernine Sedimentary Successions

The sedimentary evolution of the Amane n'Tourhart area reflects several, distinct phases, associated with different sedimentary systems.

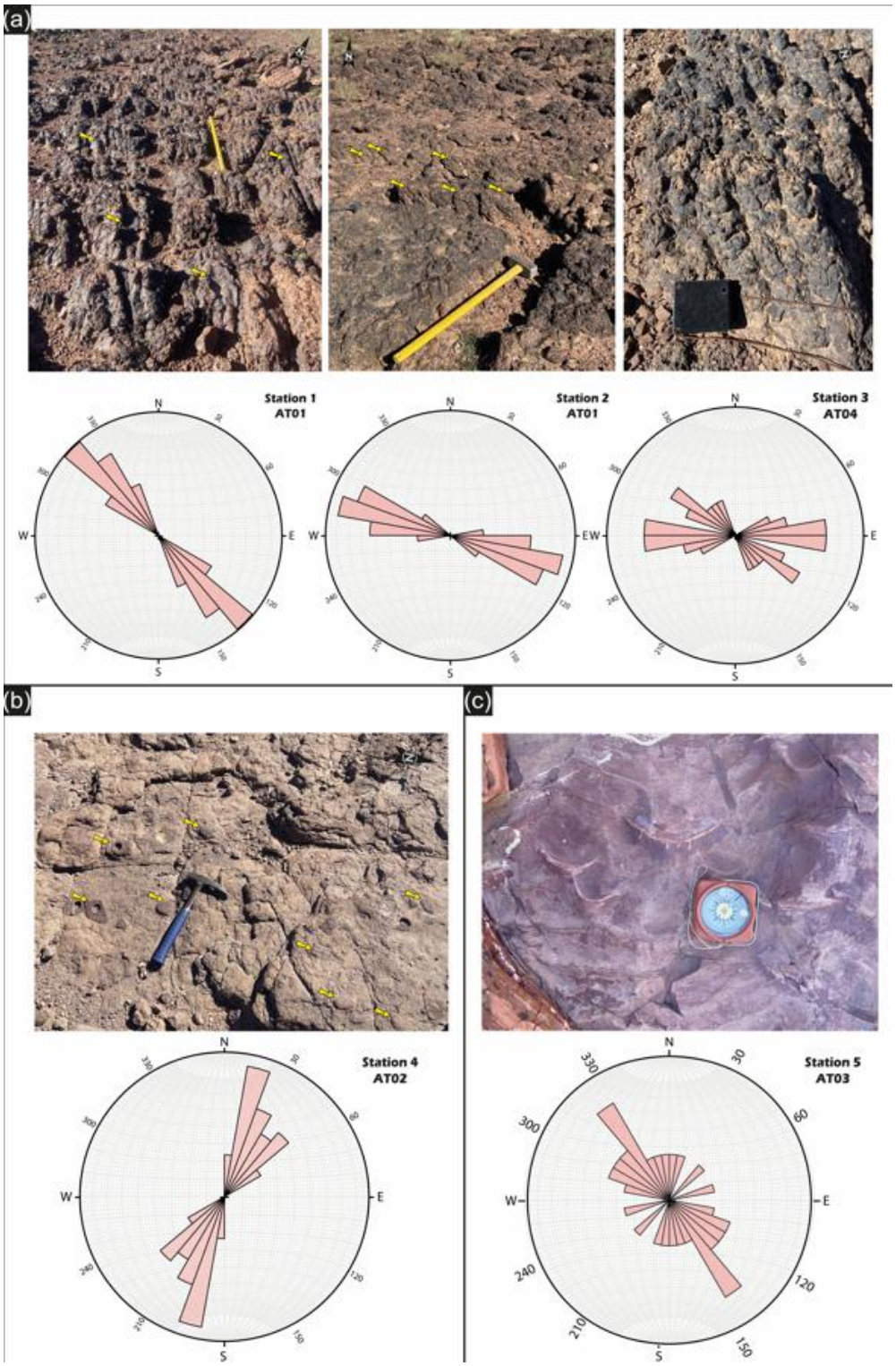

 doi:10.20944/preprints202602.0078.v1

Figure 14. (a) Inclined, columnar stromatolites with NW-SE orientation in the station 1 of the AT01 section, WNW-ESE orientation in the station 2 of the AT01 section, and W-E orientation in the station 3 of the AT04 section; (b) The imbrication of pebbles in the conglomerate facies shows a general NNE–SSW orientation in the AT02 section; (c) Ripple marks directions measured within the Sh facies in the section AT03.

a) Phase 1: Alluvial fan system

This phase is marked by a system of alluvial fans developed close to the major W-E fault (Figure 1 (d)). It is characterized by pebble-framework conglomerates at the base, and by massive clay-bearing siltstones containing carbonate nodules stratigraphically higher (Figure 15 (a)). Siliciclastic deposits are organized into channels and truncated unstratified and stratified sequences with decreasing grain size, reflecting emplacement by active alluvial systems. The imbrication of pebbles and cross-bedding observed in the conglomerates indicate a paleoflow direction oriented NNE-SSW (Figure 14 (b)). The conglomerates were deposited in a channel environment, while the massive clay-rich siltstones with carbonate nodules were formed in calmer, more extensive environments, interpreted as floodplains.

b) Phase 2: Fluviolacustrine system

This phase is marked by a gradual transition from fluvial siliciclastic deposition, represented by clay-rich siltstones with limestone nodules, to carbonate deposition, such as nodular limestones and limestones with scattered pebbles (Figure 15 (b)). This stratigraphic trend reflects a gradual decrease in fluvial influence and the emergence of a lacustrine water body, evolving from a relatively agitated to a calmer environment. All these deposits correspond to a fluviolacustrine, transitional environment that gradually evolved into a shallow-water, lacustrine system.

c) Phase 3: Shallow-water, lacustrine system

This phase corresponds to an expansion of the lacustrine system, marked by deposition of nodular to massive limestones, corresponding to depositional conditions in a relatively calm, moderately deep water-column (Figure 15 (c)). Abundant presence of stromatolites suggests local, microbially mediated carbonate deposition. The paucity of siliciclastic material suggests a protected and stable nature of this lacustrine environment.

d) Phase 4: Fluviolacustrine system

This phase is characterized by significant detrital input, combined with absent or very limited carbonate precipitation (Figure 15 (d)). These ripples show a preferred NW–SE crest orientation (Fig. 14 (c)); however, they are predominantly symmetrical to weakly asymmetrical, and measurements were therefore made along ripple crests rather than as flow-direction vectors. Their morphology indicates low-energy traction currents or wave-influenced flows in shallow water, rather than strongly unidirectional fluvial currents.

Silicified stromatolites were also deposited during this phase; they contain red, detrital laminae, far more abundant than the white, carbonate laminae.

These stromatolites reflect a dynamic evolution of the environment:

- First, in association with a strong fluvial current, small, inclined columnar stromatolites were formed with orientations NW–SE, WNW–ESE, and W–E, indicating a paleoflow shifting from NW toward W (Figure 14 (a)). This alignment is interpreted as hydrodynamically controlled, reflecting persistent shallow-water circulation within the fluviolacustrine system, rather than aeolian processes. An aeolian origin is unlikely given (i) the subaqueous facies association, (ii) the absence of diagnostic aeolian sedimentary structures, and (iii) the close spatial and stratigraphic relationship between stromatolites and ripple-bearing siliciclastic beds.
- Subsequently, a decrease in hydrodynamic energy led to a calmer environment, conducive to the formation of well-developed, vertical domal stromatolites (Figure 9. (e) – (g)).

e) Phase 5: Alluvial fan system

This final phase of sedimentary deposition is characterized by the development of an alluvial fan system, represented mainly by conglomerates and, more rarely, sandstones (Figure 14 (e)). It

 doi:10.20944/preprints202602.0078.v1

reflects a resumption of coarse-grained, detrital input, marking the terminal phase of the sedimentary system before the return to volcanic activity.

In contrast, in the Tifernine area, sedimentation is dominated by a single depositional system: lacustrine system, like the phase 3 of the Amane n'Tourhart area (Figure 15. (c)), associated with a very shallow water-column. Shallow water-depth is indicated by the presence of clay laminae accompanied by micro-conglomerates, elephant skin structure, and mud cracks; evidence for repeated emersion and associated water-escape structures. The laminar limestones locally contain thin (millimetric to centimetric) sandstone beds. These laminar limestone beds are interbedded with clay-rich siltstones containing carbonate concretions. Imbrication in micro-conglomerates indicates a weak W-E paleo-flow.

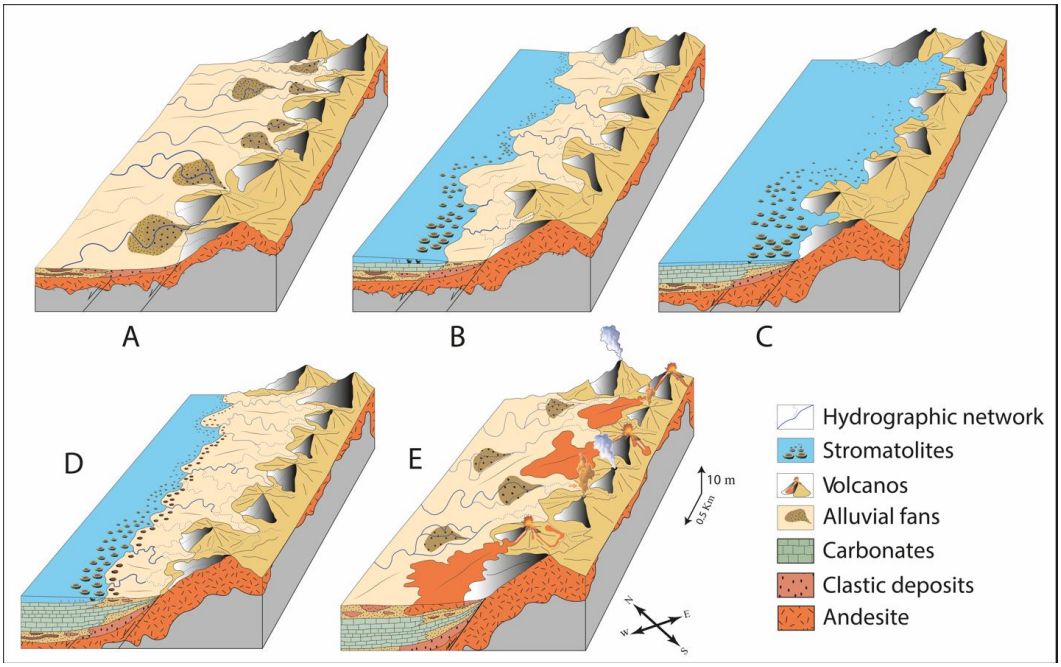

Figure 15. 3D diagrams illustrating depositional evolution of the Amane n'Tourhart sedimentary system; (a) First-stage alluvial fan; (b) First fluviolacustrine stage; (c) Lacustrine carbonate deposition; (d) Second fluvio-lacustrine stage with stromatolite growth; (e) Second alluvial fan stage marked by volcano-sedimentary (peperitic) facies and renewed volcanic activity.

Factors that controlled fluviolacustrine deposition:

Changes in the lithology of the deposits, reflecting changes in the depositional environment or sediment inputs, can be linked to external controlling factors. Sedimentation of the fluviolacustrine deposits at the Amane n'Tourhart area and lacustrine deposits at the Tifernine area was influenced by several key factors, such as climate, and volcanic activity.

5.1. Sedimentary Deposits in the Amane n'Tourhart and Tifernine Areas

The geodynamic setting of the two study areas is linked to a volcanic caldera in which the Ouarzazate Group was deposited. In the Amane n'Tourhart area, sedimentary deposits vary according to the type of sedimentary system. Alluvial-fan deposits are dominated by conglomerates, including locally derived andesitic boulders and imbricated sandstone pebbles with a more distal source. Fluviolacustrine deposits consist mainly of quartz, plagioclase, and occasional andesite fragments derived from underlying volcanic units [17,19,54]. Carbonate intervals formed in relatively low-relief, lacustrine settings, where gentle topography allowed water to pond and remain stagnant long enough for chemical precipitation to occur. In these flattened areas, detrital influx was limited, preventing dilution of carbonate minerals, while warm climatic conditions enhanced chemical weathering of the surrounding volcanic rocks, supplying the necessary ions for carbonate formation.

 doi:10.20944/preprints202602.0078.v1

Carbonate sediments subsequently underwent early- and late-stage silicification, with silica precipitating from hydrothermal fluids both at the sediment–water interface and in fractures and pores [22].

In contrast, the Tifernine area is largely characterized by carbonates chemically deposited in a lacustrine setting, with Ca^{2+} derived from the alteration of underlying volcanic rocks [104,105]. Detrital input was minimal, reflecting an environment dominated by chemical weathering rather than siliciclastic influx. Álvaro et al. [20] inferred that the Tifernine succession is older than the Amane n'Tourhart succession, based on lithostratigraphic correlation; however, U–Pb geochronology by Oukhro et al. [40] indicated that the Amane n'Tourhart succession is slightly younger, ca. 561–564 Ma, with the Tifernine succession older than ca. 566 Ma, consistent with the Bou Azzer regional mapping [57].

5.2. Climatic Control on Fluviolacustrine Deposition

Sedimentary systems in the Amane n'Tourhart and Tifernine areas has been strongly influenced by paleoclimatic conditions, which imposed a strong control on the nature of deposits, sedimentary dynamics, as well as weathering and precipitation.

Alluvial fans: arid to semi-arid climate:

Deposits associated with alluvial fans were formed under arid to semi-arid climatic conditions, favorable for the development of ephemeral water courses. This climatic framework, characterized by episodic torrential rainfall, favored physical weathering resulting in abundant production of coarse debris and torrential floods [100]. The predominance of siltstone-mudstone facies reflects mudflows.

Fluviolacustrine systems: alternating humidity and aridity:

Fluviolacustrine deposits alternate between terrigenous and chemical or biochemical sedimentation. Carbonate intervals (nodular and massive limestones) were formed under a hot and wet climate, conducive to alteration of volcanic rocks and the enrichment of runoff water in cations, promoting precipitation of calcium carbonate in the basin, particularly in the Amane n'Tourhart area [104,105]. Conversely, periods marked by a cessation or reduction in carbonate precipitation coincided with more arid climatic conditions. These periods are reflected sedimentologically with an increase in detrital input, as well as by the establishment of alluvial fans. These deposits indicate an episodic intensification of erosion in watersheds, linked to torrential rainstorms [100,106].

Tifernine area: the imprint of a hot and wet, and then dry climate:

In the Tifernine area, laminar limestone deposits indicate an initial period of hot and wet climate that favored alteration of caldera and post-caldera volcanic rocks and released cations to runoff water. These waters, also enriched with CO_2 of volcanic and/or atmospheric origin, led to the precipitation of carbonates in the basin. The overlying sedimentary record indicates a progressive lowering of the water table, with sedimentary structures such as mud cracks, pellets, elephant skin, and MISS. These structures reflect significant evaporation and insufficient runoff to compensate for water loss, indicating a transition to a drier climate.

5.3. Volcanic Control on Fluviolacustrine Deposition

In the context of the Amane n'Tourhart and Tifernine sedimentary successions, volcanic activity elsewhere in the caldera provided volcaniclastic material that fed alluvial fans and channels, changing topography and the way sediment was delivered to lakes. Between eruptions, the depositional system switched to fluviolacustrine processes, allowing fine carbonate and microbial facies to develop. This interplay can explain transition from conglomerates and sandstones deposited in braided alluvial fans to carbonate muds and stromatolitic limestones deposited in lacustrine setting. Volcanic pulses drove supply of coarse-grained material and development of alluvial fans, while quiescent periods enabled lake expansion and deposition of carbonates and microbial activity. Therefore, volcanism in these settings was not a second-order factor, but an integral forcing mechanism intertwined with tectonics and climate. It dictated sediment supply, basin

 doi:10.20944/preprints202602.0078.v1

morphodynamics, hydrology, chemistry, and facies evolution. Recognizing its role enables a more nuanced interpretation of stratigraphic architecture. Rather than treating volcanic facies as simply 'contaminants', they should be viewed as essential agents of a depositional system reorganization. Volcanic eruptions in the caldera were contemporary with deposition of fluviolacustrine, carbonate deposits in the two areas studied [21,40]. This volcanism could have enriched surface waters with dissolved inorganic carbon of magmatic origin. In addition, alteration of volcanic minerals released Ca^{2+}, and other cations like Mg^{2+} and Na^{+}, contributing to carbonate precipitation in lacustrine environments [104,105]. Volcanism also brought stromatolite growth to an end. Following deposition of the stromatolitic facies Ls1, Ls2, and Ls3, magma (Gmm1 and Gmc), containing still-hot, fresh andesitic fragments intruded into unlithified sediments, curtailing microbial ecosystem in the Amane n'Tourhart area. This event marks a renewed volcanism, followed by an emplacement of andesitic breccia flows.

6. Conclusion

The lithostratigraphic, sedimentological, and petrographic investigations carried out in the Amane n'Tourhart and Tifernine areas document the evolution of fluviolacustrine systems developed within pre- to post-caldera continental basin during the Ediacaran. Thirteen sedimentary facies were identified and grouped into four depositional assemblages (siliciclastic, carbonate, mixed siliciclastic–carbonate, and volcanic), allowing reconstruction of the spatial and temporal evolution of depositional environments from proximal fluvial domains to fully lacustrine settings.

In the Amane n'Tourhart area, the sedimentary succession records a progressive environmental transition marked by a clear vertical organization of facies. The basal coarse-grained deposits reflect high-energy fluvial conditions associated with significant topographic gradients inherited from the volcanic landscape. These deposits are overlain by mixed siliciclastic–carbonate facies, indicating the establishment of a fluviolacustrine system characterized by alternating clastic input and *in situ* carbonate accumulation. The upward transition to finely laminated and stromatolitic carbonates documents the development of persistent lacustrine conditions with reduced clastic supply, prolonged water residence time, and enhanced chemical and biologically mediated carbonate precipitation. This evolution reflects a gradual shift from detrital-dominated sedimentation to chemically and microbially influenced carbonate production.

The Tifernine succession exhibits a contrasting but complementary lacustrine record. It is dominated by fine-grained, laminated carbonates interbedded with thin siliciclastic layers, reflecting deposition in a shallow, low-energy lake environment. The widespread occurrence of desiccation cracks, nodular carbonates, and microbial laminations indicates repeated lake-level fluctuations and episodic subaerial exposure. These features point to hydrological instability, with alternating phases of carbonate precipitation during periods of reduced clastic input and evaporation, and siliciclastic influx during short-lived runoff events.

Volcanism exerted a fundamental influence on sedimentation by shaping basin morphology and directly interacting with sedimentary processes. The close stratigraphic association of lacustrine carbonates with andesitic lava flows, peperites, and volcanic breccias demonstrates that sedimentation occurred contemporaneously with volcanic activity. Volcanic relief controlled sediment supply pathways and the localization of depocenters, while synvolcanic alteration processes likely enhanced the availability of calcium and dissolved inorganic carbon in lake waters, promoting carbonate supersaturation and precipitation. The persistence of carbonate sedimentation in a continental setting thus reflects the combined effects of volcanic inputs and favorable lacustrine geochemical conditions.

Climatic variability played a key role in modulating sedimentary processes at shorter timescales. The alternation between siliciclastic-dominated intervals and carbonate-rich, laminated facies reflects fluctuations in runoff intensity, precipitation regime, and evaporation rates. Periods of enhanced clastic input are interpreted as phases of episodic, high-energy runoff under relatively arid to semi-arid conditions, whereas intervals dominated by laminated and stromatolitic carbonates record more

 doi:10.20944/preprints202602.0078.v1

stable hydrological conditions with limited detrital influx and sustained microbial activity. These climatic oscillations strongly influenced lake-level dynamics, sediment supply, and the balance between physical, chemical, and biological sedimentary processes.

Overall, the Amane n'Tourhart and Tifernine successions provide a well-preserved record of Ediacaran lacustrine sedimentation in a volcanically influenced continental basin. The sedimentary architecture reflects the interplay between volcanic landscape evolution, climate-driven hydrological variability, and biologically mediated carbonate production. These successions represent an important archive of non-marine Ediacaran environments and contribute to a better understanding of carbonate factory development and lake dynamics in Ediacaran continental settings.

Acknowledgements: Most of this work, conducted as part of Jihane Ounar's PhD thesis, was carried out at the Department of Geology, Faculty of Sciences–Semlalia, Cadi Ayyad University of Marrakech; the Department of Earth and Planetary Sciences, University of California, Riverside (USA); and the Department of Earth and Planetary Sciences, Yale University, New Haven (USA). Jihane Ounar was partially supported by a doctoral studentship from the Hassan II Academy of Science and Technology through the project "Integrated study of the biosphere evolution in relation to the fluctuations of oxygen levels recorded from the Proterozoic to the Cambrian" (Leader: N. Youbi; Project No. AcadHIIST/SDU/2016-02). The authors thank Dr Alex Kovalick and Dr Charles Diamond (University of California, Riverside) for technical assistance in Riverside. Field assistance by Eliza Poggi and Dana Polomski (Yale University) is gratefully acknowledged. This work was supported by the U.S. National Science Foundation (NSF) through the collaborative research project "Co-evolution of Earth and life across the Proterozoic–Phanerozoic transition: Integrated perspectives from outcrop and drill core" (Grant 1925549 to Alan Rooney and David Evans, Yale University).

References

1. Hoffman, P.F.; Schrag, D.P. The Snowball Earth Hypothesis: Testing the Limits of Global Change. *Terra Nova* 2002, *14*, 129–155, doi:10.1046/J.1365-3121.2002.00408.X;SUBPAGE:STRING:FULL.
2. Knoll, A.H.; Walter, M.R.; Narbonne, G.M.; Christie-Blick, N. The Ediacaran Period: A New Addition to the Geologic Time Scale. *Lethaia* 2006, *39*, 13–30, doi:10.1080/00241160500409223;WGROUP:STRING:PUBLICATION.
3. Shields-Zhou, G. The Case for a Neoproterozoic Oxygenation Event: Geochemical Evidence and Biological Consequences. *GSA TODAY* 2011, doi:10.1130/GSATG102A.1.
4. Hoffman, P.F.; Abbot, D.S.; Ashkenazy, Y.; Benn, D.I.; Brocks, J.J.; Cohen, P.A.; Cox, G.M.; Creveling, J.R.; Donnadieu, Y.; Erwin, D.H.; et Fairchild, I. J., Ferreira, D., Goodman, J. C., Halverson, G. P., Jansen, M. F., Le Hir, G., Love, G. D., Macdonald, F. A., Maloof, A. C., Partin, C. A., Ramstein, G., Rose, B. E. J., Rose, C. V., Sadler, P. M., Tziperman, E., Voigt, A., Warren, S. Gal. Snowball Earth Climate Dynamics and Cryogenian Geology-Geobiology. *Sci. Adv.* 2017, *3*, doi:10.1126/SCIADV.1600983;REQUESTEDJOURNAL:JOURNAL:SCIADV;WGROUP:STRING:PUBLICATION.
5. Xiao, S.H.; Narbonne, G.M. The Ediacaran Period. *Geologic Time Scale 2020* 2020, 521–561, doi:10.1016/B978-0-12-824360-2.00018-8.
6. Narbonne, G.M. The Ediacara Biota: Neoproterozoic Origin of Animals and Their Ecosystems. *Annu. Rev. Earth Planet. Sci.* 2005, *33*, 421–442, doi:10.1146/ANNUREV.EARTH.33.092203.122519.
7. Xiao, S.; Laflamme, M. On the Eve of Animal Radiation: Phylogeny, Ecology and Evolution of the Ediacara Biota. *Trends Ecol. Evol.* 2009, *24*, 31–40, doi:10.1016/j.tree.2008.07.015.
8. Erwin, D.H.; Laflamme, M.; Tweedt, S.M.; Sperling, E.A.; Pisani, D.; Peterson, K.J. The Cambrian Conundrum: Early Divergence and Later Ecological Success in the Early History of Animals. *Science (1979).* 2011, *334*, 1091–1097, doi:10.1126/SCIENCE.1206375;PAGE:STRING:ARTICLE/CHAPTER.
9. Hoffman, P.F.; Kaufman, A.J.; Halverson, G.P.; Schrag, D.P. A Neoproterozoic Snowball Earth. *Science (1979).* 1998, *281*, 1342–1346, doi:10.1126/SCIENCE.281.5381.1342.

 doi:10.20944/preprints202602.0078.v1

10. Halverson, G.P.; Hoffman, P.F.; Schrag, D.P.; Maloof, A.C.; Rice, A.H.N. Toward a Neoproterozoic Composite Carbon-Isotope Record. *Bulletin of the Geological Society of America* 2005, *117*, 1181–1207, doi:10.1130/B25630.1.
11. Halverson, G.P.; Wade, B.P.; Hurtgen, M.T.; Barovich, K.M. Neoproterozoic Chemostratigraphy. *Precambrian Res.* 2010, *182*, 337–350, doi:10.1016/J.PRECAMRES.2010.04.007.
12. Xiao, S.; Narbonne, G.M.; Zhou, C.; Laflamme, M.; Grazhdankin, D. V.; Moczydlowska-Vidal, M.; Cui, H. Towards an Ediacaran Time Scale: Problems, Protocols, and Prospects. *Episodes Journal of International Geoscience* 2016, *39*, 540–555, doi:10.18814/EPIIUGS/2016/V39I4/103886.
13. El Kabouri, J.; Errami, E.; Becker-Kerber, B.; Ennih, N.; Linnemann, U.; Fellah, C.; Triantafyllou, A. Ediacaran Biota from Ougnat Massif (Eastern Anti-Atlas, Morocco): Paleoenvironmental and Stratigraphic Constraints. *Journal of African Earth Sciences* 2023, *198*, 104806, doi:10.1016/J.JAFREARSCI.2022.104806.
14. El Kabouri, J, E.K.; Errami, E.; Becker-Kerber, B.; Ennih, N.; Youbi, N. Microbially Induced Sedimentary Structures from the Ediacaran of Anti-Atlas, Morocco. *Precambrian Res.* 2023, *395*, 107135, doi:10.1016/J.PRECAMRES.2023.107135.
15. El Kabouri, J.; Triantafyllou, A.; Errami, E.; Belkacim, S.; Calassou, E.; Zouicha, A.; Linnemann, U. Revising the Lithostratigraphic Framework of the Ediacaran Succession of the Anti-Atlas Belt: Correlation across the Cadomian Domain of the West African Craton. *Journal of African Earth Sciences* 2025, *229*, 105696, doi:10.1016/J.JAFREARSCI.2025.105696.
16. Beraaouz, E.H.; El Kabouri, J. First Evidence of Tubular Fossils from the Anti-Atlas: Insights into the Paleogeography of Late Ediacaran Tubular Fossils and the Ediacaran–Cambrian Boundary in the Anti-Atlas. *Precambrian Res.* 2025, *431*, 107962, doi:10.1016/J.PRECAMRES.2025.107962.
17. Choubert, G.; Hindermeyer, J.; Hollard, H. *Note Préliminaire Sur Les Collenia de l'Anti-Atlas.*; LBI.; 1952;
18. Choubert, G. *Histoire Géologique Du Domaine de l'Anti-Atlas.*; Service Géologique Maroc, Ed.; Notes Némoires.; 1952; Vol. 100;.
19. Choubert, G. *Livret-Guide de l'excursion Anti-Atlas Occidental et Central*; Service géologique du Maroc, Ed.; 1970; Vol. 229;.
20. Álvaro, J.J. ; Ezzouhairi, H. ; Ayad, N.A. ; Charif, A. ; Solá, R. ; Ribeiro, M.L. Alkaline Lake Systems with Stromatolitic Shorelines in the Ediacaran Volcanosedimentary Ouarzazate Supergroup, Anti-Atlas, Morocco. *Precambrian Res.* 2010, *179*, 22–36, doi:10.1016/J.PRECAMRES.2010.02.009.
21. Walsh, G.J. ; Benziane, F. ; Aleinikoff, J.N. ; Harrison, R.W. ; Yazidi, A. ; Burton, W.C. ; Quick, J.E. ; Saadane, A. Neoproterozoic Tectonic Evolution of the Jebel Saghro and Bou Azzer—El Graara Inliers, Eastern and Central Anti-Atlas, Morocco. *Precambrian Res.* 2012, *216–219*, 23–62, doi:10.1016/J.PRECAMRES.2012.06.010.
22. Álvaro, J.J.; González-Acebrón, L. Sublacustrine Hydrothermal Seeps and Silicification of Microbial Bioherms in the Ediacaran Oued Dar'a Caldera, Anti-Atlas, Morocco. *Sedimentology* 2019, *66*, 2048–2071, doi:10.1111/SED.12568;JOURNAL:JOURNAL:13653091;SUBPAGE:STRING:ACCESS.
23. Beraaouz, M.; Abioui, M.; Patranabis-Deb, S. Precambrian (Ediacaran) Stromatolites in the Amane-n'Tourhart (Anti-Atlas, Morocco). *International Journal of Earth Sciences 2019 108:4* 2019, *108*, 1273–1274, doi:10.1007/S00531-019-01690-1.
24. Chraiki, I.; Bouougri, E.H.; Chi Fru, E.; Lazreq, N.; Youbi, N.; Boumehdi, A.; Aubineau, J.; Fontaine, C.; El Albani, A. A 571 Million-Year-Old Alkaline Volcanic Lake Photosynthesizing Microbial Community, the Anti-Atlas, Morocco. *Geobiology* 2021, *19*, 105–124, doi:10.1111/GBI.12425;SUBPAGE:STRING:ABSTRACT;WEBSITE:WEBSITE:PERICLES;JOURNAL:JOURNAL:14724669;WGROUP:STRING:PUBLICATION.
25. Chraiki, I.; Bouougri, E.H.; El Albani, A. Microbialites Diversity from the Ediacaran of the Anti-Atlas (Morocco): A Snapshot of Microbial Oases Thriving in an Alkaline Volcanic Lake. *Annales de Paléontologie* 2022, *108*, 102584, doi:10.1016/J.ANNPAL.2022.102584.
26. Chraiki, I.; Chi Fru, E.; Somogyi, A.; Bouougri, E.H.; Bankole, O.; Ghnahalla, M.; El Albani, A. Blooming of a Microbial Community in an Ediacaran Extreme Volcanic Lake System. *Scientific Reports 2023 13:1* 2023, *13*, 9080-, doi:10.1038/s41598-023-36031-5.

 doi:10.20944/preprints202602.0078.v1

27. Carrizo, D.; Beraaouz, M.; Hssaisoune, M.; Sánchez-García, L.; Prieto-Ballesteros, O.; Parro, V. Contrasted Detection of Lipid Biomarkers in Ediacaran Stromatolites from Amane-n'Tourhart in the Moroccan Anti-Atlas. *Geoscience Frontiers* 2026, 102251, doi:10.1016/J.GSF.2026.102251.
28. Gouiza, M.; Hall, J.; Welford, J.K. Tectono-Stratigraphic Evolution and Crustal Architecture of the Orphan Basin during North Atlantic Rifting. *International Journal of Earth Sciences 2016 106:3* 2017, *106*, 917–937, doi:10.1007/S00531-016-1341-0.
29. Missenard, Y.; Zeyen, H.; de Lamotte, D.F.; Leturmy, P.; Petit, C.; Sébrier, M.; Saddiqi, O. Crustal versus Asthenospheric Origin of Relief of the Atlas Mountains of Morocco. *J. Geophys. Res. Solid Earth* 2006, *111*, doi:10.1029/2005JB003708.
30. Choubert, G.; Faure-Muret, A. 1. Anti-Atlas (Morocco). *Earth. Sci. Rev.* 1980, *16*, 87–113, doi:10.1016/0012-8252(80)90035-5.
31. Thomas, R.J.; Chevallier, L.P.; Gresse, P.G.; Harmer, R.E.; Eglington, B.M.; Armstrong, R.A.; De Beer, C.H.; Martini, J.E.J.; De Kock, G.S.; Macey, P.H.; Ingram, B. A. Precambrian Evolution of the Sirwa Window, Anti-Atlas Orogen, Morocco. *Precambrian Res.* 2002, *118*, 1–57, doi:10.1016/S0301-9268(02)00075-X.
32. Soulaimani, A.; Bouabdelli, M.; Piqué, A. The Upper Neoproterozoic-Lower Cambrian Continental Extension in the Anti-Atlas (Morocco). *Bulletin de la Société Géologique de France* 2003, *174*, 83–92, doi:10.2113/174.1.83.
33. Gasquet, D. ; Ennih, N. ; Liégeois, J.P. ; Soulaimani, A. ; Michard, A. The Pan-African Belt. *Lecture Notes in Earth Sciences* 2008, *116*, 33–64, doi:10.1007/978-3-540-77076-3_2.
34. Thomas, R.J.; Fekkak, A.; Ennih, N.; Errami, E.; Loughlin, S.C.; Gresse, P.G.; Chevallier, L.P.; Liégeois, J.P. A New Lithostratigraphic Framework for the Anti-Atlas Orogen, Morocco. *Journal of African Earth Sciences* 2004, *39*, 217–226, doi:10.1016/J.JAFREARSCI.2004.07.046.
35. Ait Lahna, A.; Youbi, N.; Tassinari, C.C.G.; Basei, M.A.S.; Ernst, R.E.; Chaib, L.; Barzouk, A.; Mata, J.; Gärtner, A.; Admou, H.; Boumehdi, M.A.; Soderland, U.; Bensalah, M.K.; Bodinier, J.; Maacha, L.; Bekker, A. Revised Stratigraphic Framework for the Lower Anti-Atlas Supergroup Based on U–Pb Geochronology of Magmatic and Detrital Zircons (Zenaga and Bou Azzer-El Graara Inliers, Anti-Atlas Belt, Morocco). *Journal of African Earth Sciences* 2020, *171*, 103946, doi:10.1016/J.JAFREARSCI.2020.103946.
36. CHOUBERT, G. *Histoire Géologique Du Précambrien de l'Anti-Atlas. (1)*; Notes Mémoires du Service Géologique du Maroc; 1963.
37. Youbi N. Le Volcanisme « Post-Collisionnel » : Un Magmatisme Intraplaque Relié à Des Panaches Mantelliques. Etude Volcanologique et Géochimique. Exemples D" Application Dans Le Néoprotérozoïque Terminal (PIII) de L'Anti-Atlas et Le Permien Du Maroc, 1998.
38. Youbi, N.; Ernst, R.E.; Söderlund, U.; Boumehdi, M.A.; Lahna, A.A.; Gaeta Tassinari, C.; Moume, W. El; Bensalah, M.K. The Central Iapetus Magmatic Province: An Updated Review and Link with the ca. 580 Ma Gaskiers Glaciation. *Special Paper of the Geological Society of America* 2020, *544*, 35–66, doi:10.1130/2020.2544(02).
39. Mediany, M.A.; Youbi, N.; Ben Chra, M.; Moutbir, O.; Hadimi, I.; Mata, J.; Wotzlaw, J.F.; Madeira, J.; Doblas, M.; Khalaf, E.E.D.A.H.; Oukhro, R.; El Moume, W.; Ounar, J.; Ait Lahna, A.; Boumehdi, M.A.; Bekker, A. Volcanic Response to Post-Pan-African Orogeny Delamination: Insights from Volcanology, Precise U-Pb Geochronology, Geochemistry, and Petrology of the Ediacaran Ouarzazate Group of the Anti-Atlas, Morocco. *Minerals* 2025, *15*, 142, doi:10.3390/MIN15020142/S1.
40. Oukhro, R.; Youbi, N.; Kalderon-Asael, B.; Evans, D.A.D.; Pierce, J.; Wotzlaw, J.F.; Ovtcharova, M.; Mata, J.; Mediany, M.A.; Ounar, J.; El Moume, W.; Hadimi, I.; Moutbir, O.; Boumehdi, M.A.; Bekker, A. Volcanic Stratigraphy, Petrology, Geochemistry and Precise U-Pb Zircon Geochronology of the Late Ediacaran Ouarzazate Group at the Oued Dar'a Caldera: Intracontinental Felsic Super-Eruptions in Association with Continental Flood Basalt Magmatism on the W…. *Minerals* 2025, *15*, 776, doi:10.3390/MIN15080776/S1.
41. Pierce, J.S.; Evans, D.A.D.; Polomski, D.E.; Youbi, N.; Mediany, M.A.; Ounar, J.; Oukhro, R.; Boumehdi, M.A.; Strauss, J. V.; Keller, C.B.; Gärtner, A.; Ovtcharova, M.; Wotzlaw, J.; Linnemann. Magnetostratigraphic Constraints on the Late Ediacaran Paleomagnetic Enigma. *Sci. Adv.* 2025, *11*, eady3258, doi:10.1126/SCIADV.ADY3258;JOURNAL:JOURNAL:SCIADV;WEBSITE:WEBSITE:AAAS-SITE;ISSUE:ISSUE:DOI.

42. Tuduri, J. ; Chauvet, A. ; Barbanson, L. ; Bourdier, J.L. ; Labriki, M. ; Ennaciri, A. ; Badra, L. ; Dubois, M. ; Ennaciri-Leloix, C. ; Sizaret, S. ; Maacha, L. The Jbel Saghro Au (–Ag, Cu) and Ag–Hg Metallogenetic Province : Product of a Long-Lived Ediacaran Tectono-Magmatic Evolution in the Moroccan Anti-Atlas. *Minerals 2018, Vol. 8, Page 592* 2018, *8*, 592, doi:10.3390/MIN8120592.
43. Doblas, M.; López-Ruiz, J.; Cebriá, J.-M.; Youbi, N.; Degroote, E. Mantle Insulation beneath the West African Craton during the Precambrian-Cambrian Transition. *Geology* 2002, *30*, 839–842.
44. Youbi, N.; Ernst, R.E.; Mitchell, R.N.; Boumehdi, M.A.; Moume, W. El; Lahna, A.A.; Bensalah, M.K.; Söderlund, U.; Doblas, M.; Tassinari, C.C.G. Preliminary Appraisal of a Correlation Between Glaciations and Large Igneous Provinces Over the Past 720 Million Years. *Large Igneous Provinces: A Driver of Global Environmental and Biotic Changes* 2021, 169–190, doi:10.1002/9781119507444.CH8;CSUBTYPE:STRING:EDITED.
45. Ennih, N.; Liégeois, J.P. The Boundaries of the West African Craton, with Special Reference to the Basement of the Moroccan Metacratonic Anti-Atlas Belt. *Geol. Soc. Spec. Publ.* 2008, *297*, 1–17, doi:10.1144/SP297.1.
46. Gasquet, D.; Levresse, G.; Cheilletz, A.; Azizi-Samir, M.R.; Mouttaqi, A. Contribution to a Geodynamic Reconstruction of the Anti-Atlas (Morocco) during Pan-African Times with the Emphasis on Inversion Tectonics and Metallogenic Activity at the Precambrian–Cambrian Transition. *Precambrian Res.* 2005, *140*, 157–182, doi:10.1016/J.PRECAMRES.2005.06.009.
47. Blein, O. ; Baudin, T. ; Chèvremont, P. ; Soulaimani, A. ; Admou, H. ; Gasquet, P. ; Cocherie, A. ; Egal, E. ; Youbi, N. ; Razin, P. ; Bouabdelli, M. ; Gombert Bouabd, P. Geochronological Constraints on the Polycyclic Magmatism in the Bou Azzer-El Graara Inlier (Central Anti-Atlas Morocco). *Journal of African Earth Sciences* 2014, *99*, 287–306, doi:10.1016/J.JAFREARSCI.2014.04.021.
48. Ousbih, M.; Ikenne, M.; Cousens, B.; Chelle-Michou, C.; El Bilali, H.; Gaouzi, A.; Markovic, S.; Askkour, F.; Mouhajir, M.; El Mouden, S.; Youbi, N.; Ernst, R.E. Stratigraphy, Geochronology, Geochemistry and Nd Isotopes of the Ouarzazate Group, Anti-Atlas, Morocco: Evidence of a Late Neoproterozoic LIP in the Northwestern Part of the West African Craton. *Lithos* 2024, *474–475*, 107593, doi:10.1016/J.LITHOS.2024.107593.
49. Walsh, G.J.; Aleinikoff, J.N.; Benziane, F.; Yazidi, A.; Armstrong, T.R. U–Pb Zircon Geochronology of the Paleoproterozoic Tagragra de Tata Inlier and Its Neoproterozoic Cover, Western Anti-Atlas, Morocco. *Precambrian Res.* 2002, *117*, 1–20, doi:10.1016/S0301-9268(02)00044-X.
50. Schiavo, A.; Taj Eddine, K.; Algouti, A.; Benvenuti, M.; Dal Piaz, G.; Eddebbi, A.; El Boukhari, A.; Laftouhi, N.; Massironi, M.; Moratti, G.; Ouanaimi, H.; Pasquaré, G.; Visona, D. Carte Geologique Du Maroc Au 1/50 000, Feuille Imtir - Notice Explicative. *Notes et Mémoires du Service Géologique du Maroc, Feuille Nord* 2007, *518bis*, 1–96.
51. Bouabdellah, M.; Maacha, L.; Levresse, G.; Saddiqi, O. The Bou Azzer Co–Ni–Fe–As (±Au ± Ag) District of Central Anti-Atlas (Morocco): A Long-Lived Late Hercynian to Triassic Magmatic-Hydrothermal to Low-Sulphidation Epithermal System. 2016, 229–247, doi:10.1007/978-3-319-31733-5_8.
52. Newhall, C.G.; Self, S. The Volcanic Explosivity Index (VEI): An Estimate of Explosive Magnitude for Historical Volcanism. *J. Geophys. Res.* 1982, *87*, 1231–1238, doi:10.1029/JC087IC02P01231;JOURNAL:JOURNAL:21562202C;PAGE:STRING:ARTICLE/CHAPTER.
53. Cas, R.A.F.; Wright, J. V. Volcanism and Tectonic Setting. *Volcanic Successions Modern and Ancient* 1988, 444–467, doi:10.1007/978-94-009-3167-1_15.
54. Raaben, M.E. Some Stromatolites of the Precambrian of Morocco. *Earth. Sci. Rev.* 1980, *16*, 221–234, doi:10.1016/0012-8252(80)90043-4.
55. Landing, E.; Geyer, G.; Heldmaier, W. Distinguishing Eustatic and Epeirogenic Controls on Lower-Middle Cambrian Boundary Successions in West Gondwana (Morocco and Iberia). *Sedimentology* 2006, *53*, 899–918, doi:10.1111/J.1365-3091.2006.00780.X;PAGE:STRING:ARTICLE/CHAPTER.
56. Blein, O. ; Chèvremont, P. ; Razin, P. ; Baudin, T. ; Gasquet, D. Carte Géologique Du Maroc (1/50 000), Feuille de Bou Azer. *Notes et Mémoires du Service Géologique* 2013.
57. Chèvremont, P. ; Blein, O. ; Razin, P. ; Baudin, T. ; Barbanson, L. ; Gasquet, D. ; Soulaimani, A. ; Admou, H. ; Youbi, N. ; Bouabdelli, M. ; Anzar-Conseil. *Notice Explicative Carte Géologique Maroc (1/50 000), Feuille de Bou Azer*; Service Géologique. ; 2013 ; Vol. 535 ;

58. Busby-Spera, C.J.; White, J.D.L. Variation in Peperite Textures Associated with Differing Host-Sediment Properties. *Bull. Volcanol.* 1987, *49*, 765–776, doi:10.1007/BF01079827/METRICS.
59. White, J.D.L.; McPhie, J.; Skilling, I. Peperite: A Useful Genetic Term. *Bull. Volcanol.* 2000, *62*, 65–66.
60. Skilling, I.P.; White, J.D.L.; McPhie, J. Peperite: A Review of Magma–Sediment Mingling. *Journal of Volcanology and Geothermal Research* 2002, *114*, 1–17, doi:10.1016/S0377-0273(01)00278-5.
61. Miall, A.D. The Stratigraphic Architecture of Fluvial Depositional Systems. *The Geology of Fluvial Deposits* 1996, 251–309, doi:10.1007/978-3-662-03237-4_9.
62. Platt, N.H.; Wright, V.P. Palustrine Carbonates and the Florida Everglades; towards an Exposure Index for the Fresh-Water Environment? *Journal of Sedimentary Research* 1992, *62*, 1058–1071, doi:10.1306/D4267A4B-2B26-11D7-8648000102C1865D.
63. Alonso-Zarza, A.M.; Wright, V.P. Chapter 2 Palustrine Carbonates. *Developments in Sedimentology* 2010, *61*, 103–131, doi:10.1016/S0070-4571(09)06102-0.
64. Miall, A.D. Fluvial Sedimentology: An Historical Review. *Dallas Geological Society* 1977, 1–47.
65. Collinson, J.D. Alluvial Sediments. Sedimentary Environments: Processes, Facies, and Stratigraphy. *Blackwell Scientific Publications* 1996, *49*, 37–82, doi:10.4116/JAQUA.49.201.
66. Ghazi, S.; Mountney, N.P. Facies and Architectural Element Analysis of a Meandering Fluvial Succession: The Permian Warchha Sandstone, Salt Range, Pakistan. *Sediment. Geol.* 2009, *221*, 99–126, doi:10.1016/J.SEDGEO.2009.08.002.
67. Ubeid, K.F. Quaternary Alluvial Deposits of Wadi Gaza in the Middle of the Gaza Strip (Palestine): Facies, Granulometric Characteristics, and Their Paleoflow Direction. *Journal of African Earth Sciences* 2016, *118*, 274–283, doi:10.1016/J.JAFREARSCI.2016.03.012.
68. Scherer, C.M.S.; Lavina, E.L.C.; Dias Filho, D.C.; Oliveira, F.M.; Bongiolo, D.E.; Aguiar, E.S. Stratigraphy and Facies Architecture of the Fluvial–Aeolian–Lacustrine Sergi Formation (Upper Jurassic), Recôncavo Basin, Brazil. *Sediment. Geol.* 2007, *194*, 169–193, doi:10.1016/J.SEDGEO.2006.06.002.
69. Fisher, J.A.; Nichols, G.J.; Waltham, D.A. Unconfined Flow Deposits in Distal Sectors of Fluvial Distributary Systems: Examples from the Miocene Luna and Huesca Systems, Northern Spain. *Sediment. Geol.* 2007, *195*, 55–73, doi:10.1016/J.SEDGEO.2006.07.005.
70. Harms, J.C.; Southard, J.B.; Southard, J.B.; Walker, R.G. Structures and Sequences in Clastic Rocks. *SEPM Society for Sedimentary Geology* 1982, *9*, doi:10.2110/SCN.82.09.
71. Arnott, R.W.C.; Hand, B.M. Bedforms, Primary Structures and Grain Fabric in the Presence of Suspended Sediment Rain. *Journal of Sedimentary Research* 1989, *59*, 1062–1069, doi:10.1306/212F90F2-2B24-11D7-8648000102C1865D.
72. Chen, L.; Steel, R.J.; Guo, F.; Olariu, C.; Gong, C. Alluvial Fan Facies of the Yongchong Basin: Implications for Tectonic and Paleoclimatic Changes during Late Cretaceous in SE China. *J. Asian Earth Sci.* 2017, *134*, 37–54, doi:10.1016/J.JSEAES.2016.10.010.
73. Miall, A.D. Lithofacies Types and Vertical Profile Models in Braided River Deposits: A Summary. *Dallas Geological Society* 1977, 597–604.
74. Ghibaudo, G. Subaqueous Sediment Gravity Flow Deposits: Practical Criteria for Their Field Description and Classification. *Sedimentology* 1992, *39*, 423–454, doi:10.1111/J.1365-3091.1992.TB02126.X;PAGE:STRING:ARTICLE/CHAPTER.
75. Garcia-Ruiz, J.M. Geochemical Scenarios for the Precipitation of Biomimetic Inorganic Carbonates. *SEPM Society for Sedimentary Geology* 2000.
76. Beck, R.; Andreassen, J.P. Spherulitic Growth of Calcium Carbonate. *Cryst. Growth Des.* 2010, *10*, 2934–2947, doi:10.1021/CG901460G.
77. Meister, P.; Johnson, O.; Corsetti, F.; Nealson, K.H. Magnesium Inhibition Controls Spherical Carbonate Precipitation in Ultrabasic Springwater (Cedars, California) and Culture Experiments. *Lecture Notes in Earth Sciences* 2011, *131*, 101–121, doi:10.1007/978-3-642-10415-2_6.
78. Last, W.M. Lacustrine Dolomite—an Overview of Modern, Holocene, and Pleistocene Occurrences. *Earth. Sci. Rev.* 1990, *27*, 221–263, doi:10.1016/0012-8252(90)90004-F.
79. Gierlowski-Kordesch, E.H. Chapter 1 Lacustrine Carbonates. *Developments in Sedimentology* 2010, *61*, 1–101, doi:10.1016/S0070-4571(09)06101-9.

80. Wright, V.P.; Barnett, A.J. An Abiotic Model for the Development of Textures in Some South Atlantic Early Cretaceous Lacustrine Carbonates. *Geol. Soc. Spec. Publ.* 2015, *418*, 209–219, doi:10.1144/SP418.3.
81. Riding, R. Microbial Carbonates: The Geological Record of Calcified Bacterial-Algal Mats and Biofilms. *Sedimentology* 2000, *47*, 179–214, doi:10.1046/J.1365-3091.2000.00003.X;REQUESTEDJOURNAL:JOURNAL:13653091;WGROUP:STRING:PUBLICATION.
82. Dupraz, C.; Visscher, P.T. Microbial Lithification in Marine Stromatolites and Hypersaline Mats. *Trends Microbiol.* 2005, *13*, 429–438, doi:10.1016/j.tim.2005.07.008.
83. Freytet, P.; Verrecchia, E.P. Freshwater Organisms That Build Stromatolites: A Synopsis of Biocrystallization by Prokaryotic and Eukaryotic Algae. *Sedimentology* 1998, *45*, 535–563, doi:10.1046/J.1365-3091.1998.00155.X.
84. Alonso-Zarza, A.M. Palaeoenvironmental Significance of Palustrine Carbonates and Calcretes in the Geological Record. *Earth. Sci. Rev.* 2003, *60*, 261–298, doi:10.1016/S0012-8252(02)00106-X.
85. Wright, V.P. Syngenetic Formation of Grainstones and Pisolites from Fenestral Carbonates in Peritidal Settings: DISCUSSION. *Journal of Sedimentary Research* 1990, *60*, 309–310.
86. Patt, N.H. Lacustrine Carbonates and Pedogenesis: Sedimentology and Origin of Palustrine Deposits from the Early Cretaceous Rupelo Formation, W Cameros Basin, N Spain. *Sedimentology* 1989, *36*, 665–684, doi:10.1111/J.1365-3091.1989.TB02092.X;WGROUP:STRING:PUBLICATION.
87. Freytet, P.; Verrecchia, E.P. Lacustrine and Palustrine Carbonate Petrography: An Overview. *J. Paleolimnol.* 2002, *27*, 221–237, doi:10.1023/A:1014263722766/METRICS.
88. Larena, Z.; Arenas, C.; Baceta, J.I.; Murelaga, X.; Suarez-Hernando, O. Stratigraphy and Sedimentology of Distal-Alluvial and Lacustrine Deposits of the Western-Central Ebro Basin (NE Iberia) Reflecting the Onset of the Middle Miocene Climatic Optimum. *Geologica acta* 2020, *18*, 1–26, doi:10.1344/GEOLOGICAACTA2020.18.7.
89. Noffke, N.; Gerdes, G.; Klenke, T.; Krumbein, W.E. Microbially Induced Sedimentary Structures: A New Category within the Classification of Primary Sedimentary Structures. *Journal of Sedimentary Research* 2001, *71*, 649–656, doi:10.1306/2DC4095D-0E47-11D7-8643000102C1865D.
90. Noffke, N.; Gerdes, G.; Klenke, T.; Krumbein, W.E. Microbially Induced Sedimentary Structures Indicating Climatological, Hydrological and Depositional Conditions within Recent and Pleistocene Coastal Facies Zones (Southern Tunisia). *Facies 2001 44:1* 2001, *44*, 23–30, doi:10.1007/BF02668164.
91. Noffke, N.; Gerdes, G.; Klenke, T. Benthic Cyanobacteria and Their Influence on the Sedimentary Dynamics of Peritidal Depositional Systems (Siliciclastic, Evaporitic Salty, and Evaporitic Carbonatic). *Earth. Sci. Rev.* 2003, *62*, 163–176, doi:10.1016/S0012-8252(02)00158-7.
92. Noffke, N. Turbulent Lifestyle: Microbial Mats on Earth's Sandy Beaches—Today and 3 Billion Years Ago. *GSA Today* 2008, *18*, 4–9, doi:10.1130/GSATG7A.1.
93. Noffke, N. The Criteria for the Biogeneicity of Microbially Induced Sedimentary Structures (MISS) in Archean and Younger, Sandy Deposits. *Earth. Sci. Rev.* 2009, *96*, 173–180, doi:10.1016/J.EARSCIREV.2008.08.002.
94. Noffke, N. *Geobiology: Microbial Mats in Sandy Deposits from the Archean Era to Today*; Springer Heidelberg.; 2010;
95. Noffke, N. Microbially Induced Sedimentary Structures in Clastic Deposits: Implication for the Prospection for Fossil Life on Mars. *Astrobiology* 2021, *21*, 866–892, doi:10.1089/AST.2021.0011.
96. Arenas-Abad, C.; Vázquez-Urbez, M.; Pardo-Tirapu, G.; Sancho-Marcén, C. Chapter 3 Fluvial and Associated Carbonate Deposits. *Developments in Sedimentology* 2010, *61*, 133–175, doi:10.1016/S0070-4571(09)06103-2.
97. Klappa, C.F. Lichen Stromatolites; Criterion for Subaerial Exposure and a Mechanism for the Formation of Laminar Calcretes (Caliche). *Journal of Sedimentary Research* 1979, *49*, 387–400, doi:10.1306/212F7752-2B24-11D7-8648000102C1865D.
98. Zhou, J.; Chafetz, H.S. The Genesis of Late Quaternary Caliche Nodules in Mission Bay, Texas: Stable Isotopic Compositions and Palaeoenvironmental Interpretation. *Sedimentology* 2009, *56*, 1392–1410, doi:10.1111/J.1365-3091.2008.01039.X;CTYPE:STRING:JOURNAL.

 doi:10.20944/preprints202602.0078.v1

99. Miller, C.R.; James, N.P. Autogenic Microbial Genesis of Middle Miocene Palustrine Ooids; Nullarbor Plain, Australia. *Journal of Sedimentary Research* 2012, *82*, 633–647, doi:10.2110/JSR.2012.60.
100. Blair, T.C.; McPherson, J.G. Processes and Forms of Alluvial Fans. *Geomorphology of Desert Environments* 2009, 413–467, doi:10.1007/978-1-4020-5719-9_14.
101. Davoudi, A.; Khodabakhsh, S.; Rafiei, B. Alluvial Fan Facies of the Qazvin Plain: Paleoclimate and Tectonic Implications during Quaternary. *Geopersia* 2020, *10*, 65–87, doi:10.22059/GEOPE.2019.277922.648469.
102. Waresback, D.B.; Turbeville, B.N. Evolution of a Plio-Pleistocene Volcanogenic-Alluvial Fan: The Puye Formation, Jemez Mountains, New Mexico. *GSA Bulletin* 1990, *102*, 298–314.
103. Amezcua, N.; Gawthorpe, R.L.; Marshall, J. Lacustrine Carbonate Lithofacies Characterization, Paleontological Content and Depositional Processes in the Mayrán Basin System. *J. South Am. Earth Sci.* 2021, *111*, 103451, doi:10.1016/J.JSAMES.2021.103451.
104. Edmonds, M.; Tutolo, B.; Iacovino, K.; Moussallam, Y. Magmatic Carbon Outgassing and Uptake of CO2 by Alkaline Waters. *American Mineralogist* 2020, *105*, 28–34, doi:10.2138/AM-2020-6986CCBY/XML.
105. Frugone-Alvarez, M.; Latorre, C.; Barreiro-Lostres, F.; Giralt, S.; Moreno, A.; Polanco-Martinez, J.; Maldonado, A.; Carrevedo, M.L.; Bernárdez, P.; Prego, R.; Huertas, A.D.; Fuentealba, M.; Valero-Garcés, B. Volcanism and Climate Change as Drivers in Holocene Depositional Dynamic of Laguna Del Maule (Andes of Central Chile - 36° S). *Climate of the Past* 2020, *16*, 1097–1125, doi:10.5194/CP-16-1097-2020.
106. Gourari, L. Etude Hydrochimique, Morphologique, Lithostratigraphique, Sédimentologique et Pétrographique Des Dépôts Travertino-Détritiques Actuels et Plio-Quaternaire Du Bassin Karstique de l'oued Aggaï (Causse de Sefrou Moyen Atlas, Maroc)., Université de Fes, 2001.